Journal of Hazardous Materials 490 (2025) 137873

Contents lists available at ScienceDirect

Journal of Hazardous Materials

journal homepage: www.elsevier.com/locate/jhazmat

An evaluation of quartz as a component of respirable coal dust

Amir Eskanlou, Barbara J. Arnold *

John and Willie Leone Family Department of Energy and Mineral Engineering, College of Earth and Mineral Science, The Pennsylvania State University, University Park, PA 16802, USA

HIGHLIGHTS

- Fresh quartz surface promotes •OH generation, especially in alkaline conditions.
- Carboxymethyl cellulose effectively reduces •OH generation of quartz.
- Surface aging decreases •OH generation of quartz.
- Quartz •OH generation varies with metal impurities like iron.
- Iron promotes H_2O_2 production on quartz in the presence of oxygen.

GRAPHICAL ABSTRACT

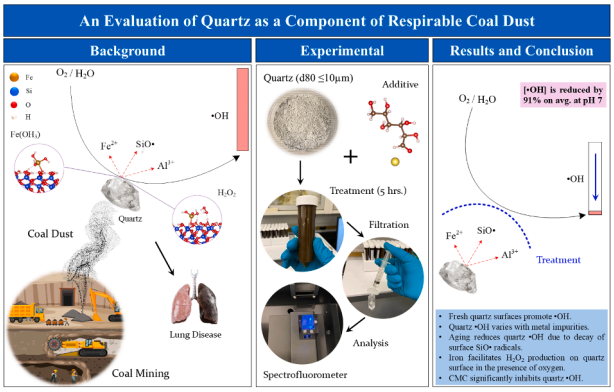

ARTICLE INFO

Keywords:
Quartz
Coal
Free radicals
Toxicity
Respirable coal dust

ABSTRACT

The rising cases of coal worker's pneumoconiosis since the early 2000s have driven research into respirable coal dust. Prolonged quartz dust exposure is deemed to be the primary cause of the resurgence in pneumoconiosis. This study examines how quartz present in coals of various ranks produces hydroxyl radicals (•OH), a reactive oxygen species linked to particle toxicity. This study evaluates the ability of safe chemical additives to reduce •OH production of the coal-quartz samples at various pH levels. Promising chemicals were investigated in different solutions, including tap and process waters and simulated lung fluid (SLF). We combined insights from electrokinetic measurements, infrared and X-ray photoelectron spectroscopies, and *ab initio* atomistic simulations to study the quartz particle surfaces. The study also explored how surface aging impacts quartz •OH production. The results reveal that •OH generation of the quartz varies and is enhanced by iron contamination, as also confirmed by *ab initio* simulations. Iron also enhances hydroxamic acid adsorption, leading to stronger interaction of the reagent on the quartz surface. Fresh quartz surfaces are particularly prone to generating more •OH in alkaline conditions. Carboxymethyl cellulose was notably effective in inhibiting quartz •OH by about 91 % at pH 7 in deionized water. The production of •OH was minimal in SLF compared to other tested solutions. The negative charge on quartz surface in various aqueous solutions was found to impact •OH generation. Quartz surface aging results in a gradual decrease in •OH generation due to the decay of surface siloxyl radicals.

* Corresponding author.
E-mail address: bja4@psu.edu (B.J. Arnold).

https://doi.org/10.1016/j.jhazmat.2025.137873
Received 26 December 2024; Received in revised form 4 March 2025; Accepted 5 March 2025
Available online 6 March 2025

1. Introduction

Despite being nearly eradicated in the 1990s, the prevalence and severity of Coal Worker's Pneumoconiosis (CWP) resurged in the early 2000s, especially in central Appalachia [1,2]. Coal mining activities produce dust containing ultrafine particles of coal and its associated components, including crystalline silica (quartz) and pyrite, among others, and sometimes diesel particulate matter (DPM) [2–4]. These particles, due to their small size (d80 <10μm, d50 ≤4μm), can reach the deeper regions of the lungs where breathing functions take place [5]. The fresh surfaces of these particles can form reactive oxygen species (ROS) like hydroxyl radicals (•OH) upon exposure to the biological fluids inside the respiratory system [6,7]. Hydroxyl radicals are widely recognized as the most reactive ROS and are primary contributors to dust toxicity and its associated harmful effects [8]. In the lungs, •OH from dust particles causes significant tissue damage by seeking electrons from lung tissues [6,9], which can be described as the dust toxicity [7, 10]. The generation of •OH radicals has also been linked to CWP [11–13], which remains a major issue in the coal mining industry, especially in central Appalachia [2, 4, 14]. Biological responses and toxicity of dust depend on its physical and chemical properties, making it essential to study coal dust components [7,10].

Quartz (SiO_2) is a major mineral component in coal dust [7,15]. It is well established that intensive exposure to quartz dust can lead to respiratory and autoimmune diseases including silicosis, rheumatoid arthritis, and lupus [16–19]. Excessive exposure to quartz has been identified as the primary cause of the resurgence in pneumoconiosis [20, 21]. An analysis of federal dust monitoring data from 1982 to 2017 shows that respirable quartz levels in mines in central Appalachia have consistently exceeded permissible exposure limits [22,23]. This has contributed to an increased prevalence of silicosis-related lesions in miners [24,25]. Furthermore, pathological studies of miners with severe forms of CWP, such as rapidly progressive pneumoconiosis (RPP) [26] and progressive massive fibrosis (PMF) [27], have highlighted features of accelerated silicosis and mixed-dust pneumoconiosis [21]. These findings indicate a more aggressive disease process than traditional CWP [2]. The new rule by the Mine Safety and Health Administration (MSHA) limits quartz dust exposure to 0.05 mg/m^3 (8-h time-weighted average concentration). This regulation indicates the maximum concentration of quartz dust that a worker can be exposed to for up to a 10-h workday during a 40-h workweek [28,29].

Quartz dust can also promote lung cancer [30,31]. The International Agency for Research on Cancer (IARC) [32] has classified quartz and cristobalite (a polymorph of crystalline silica) as Group 1 carcinogens, meaning that there is sufficient evidence that they cause cancer in humans. Experimental *in vitro* studies have shown that quartz dust exposure can damage cell membranes and DNA in alveolar macrophages [33], form ROS in lung epithelial cells, and release inflammatory cytokines [34]. According to IARC [32], the carcinogenicity and biological activity of crystalline silica may depend on the type of silica or on other factors including crystal defects, chemical functionalities, and association with other substances. The exact mechanism of •OH production on the quartz surface is not fully understood, but there are proposed mechanisms, including through the formation of SiO• radicals from disorganized silanol groups (Si-OH) on the freshly fractured quartz [35–37], in a dry oxygen environment [18,38], and through mechanical fracturing, which disrupts the arrangement of non-radical moieties on the surface leading to cellular toxicity [39,40]. Studies by Sarver *et al.* [2, 41–44] showed that quartz dust, primarily sourced from rock strata drilled for roof bolting or mined alongside coal, poses significant health risks, especially in thin-seam mining operations common in Central Appalachia. The finer silica particles identified near drilling and cutting activities exhibit higher surface reactivity, penetrating deeper into the lungs.

Much of the occupational exposure to quartz dust involves mixed dusts, such as coal dust, where the quartz surface might be altered by the presence of substances like coal, clays, iron, or aluminum [45]. Coal dust from various locations within a single mine such as the coal seam, rock dust, floor, and roof sources can exhibit different surface areas with distinct physicochemical properties and varying levels of toxicity [46]. The synergistic effects of transition metallic elements with quartz particles have been linked to high lung cancer mortality, which may be due to the enhanced carcinogenic activity of quartz dust in the presence of these elements [47]. This underscores the need to investigate the surface chemistry properties and •OH generation of quartz from various coals, which have not yet been investigated or compared in prior research. Additionally, the effects of solution pH and atmospheric surface aging on quartz particles, which could further influence their surface chemistry and health impacts, remain underexplored areas.

In this study, quartz was evaluated as a component of respirable coal dust. The generation of •OH by quartz particles can be directly related to their surface oxidation. Hence, it can be hypothesized that preventing or minimizing surface oxidation of quartz dust could lead to a reduction or elimination of •OH production in biological environments. To test this hypothesis, the surface chemistry of quartz was assessed with the aim of reducing •OH generation by applying various non-hazardous chemical additives as surface-modifying agents to both freshly generated and aged quartz dust particles. Tests were performed using deionized (DI, 18.2 MΩ·cm) water, tap water, process plant water (to simulate the water used in mine dust sprays), and simulated lung fluid (SLF) to assess the impact of ions on •OH generation. Combining the predictive power of *ab initio* molecular dynamics (AIMD) simulations with experimental observations is highly valuable for assessing surface chemistry and interfacial interactions. In this study, AIMD simulations based on density functional theory (DFT) were conducted to gain insights into atomic-level interactions on the quartz surface.

2. Materials and methods

2.1. Sample collection and preparation

Bulk samples of spiral refuse (-16M+100 M) were obtained from three coal preparation plants. They represented a High Volatile A Bituminous (HVAb) from Upper Freeport and Upper Kittanning seam coals, Medium Volatile Bituminous (MVb) from Lower Kittanning, Brookville, and Upper Kittanning seam coals, and Low Volatile Bituminous (LVb) from Upper Kittanning and minor amounts of Upper Freeport seam coals. The spiral refuse samples were processed on a laboratory concentrating table in the Penn State Mineral Processing Laboratory to provide a middling sample that contained quartz and a heavy fraction containing pyrite. Optical microscope photographs of the middling/refuse samples acquired under ambient conditions indicated that quartz particles in the samples are fully liberated, as shown in Fig. S-1-a. With such liberation and the coarse size, we were able to handpick sufficient quartz particles using laboratory thumb forceps, as shown in Fig. S-1-b. The obtained quartz samples were subjected to mineralogical phase identification characterizations using the X-ray powder diffraction (XRD) method.

Quartz dust samples were prepared using a Rocklabs® benchtop ring mill, equipped with a chrome alloy and tungsten carbide grinding bowl and media, as illustrated in Fig. S-2. For each batch, one gram of pulverized sample with an initial d_{80} of approximately 250 μm was used. The total grinding duration for each batch was 25 min, divided into 5-min intervals, with a 1-min cooling period between intervals to prevent the grinding bowl and media from overheating.

2.2. Chemicals

To investigate the effect of chemical additives in eliminating or reducing the toxicity (generation of •OH) of the quartz dust particles, nine non-hazardous chemical additives were examined. The chemical additives were selected based on their diverse mechanisms of action and

Table 1
Details of the chemical reagents examined in the current study.

Chemical	Category	Concentrations (mol. L^{-1})
Octanohydroxamic acid (OHA)	Chelating agent	1.40×10^{-3}
		2.80×10^{-3}
Carboxy methyl cellulose (CMC)	Polyanionic polymer	0.76×10^{-3}
		1.53×10^{-3}
Hydroxypropyl cellulose (HPC)	Nonionic polymer	0.62×10^{-5}
		1.24×10^{-5}
Poly(1-vinylpyrrolidone) (PVP)	Nonionic polymer	1.25×10^{-5}
		2.50×10^{-5}
Commercial Dust Suppressant A (CDS-A)	Dust suppressant	0.10 vol%
		0.20 vol%
Commercial Dust Suppressant B (CDS-B)	Dust suppressant	0.10 vol%
		0.20 vol%
Polyethylene glycol (PEG)	Nonionic polymer	1.95×10^{-4}
		3.90×10^{-4}
Commercial Dust Suppressant C (CDS-C)	Dust suppressant	1.00 vol%
		2.00 vol%
Commercial Dust Suppressant D (CDS-D)	Dust suppressant	0.15 vol%
		0.30 vol%

Table 2
Composition of the simulated lung fluid used in this study.

Chemical	CAS
Sodium bicarbonate	144–55–8
Sodium acetate	127–09–3
Calcium chloride dihydrate	10,035–04–8
Potassium chloride	7440–09–7
Magnesium chloride	7786–30–3
Sodium Sulphate	7757–82–6
Sodium chloride	7440–23–5
Sodium citrate dihydrate	6132–04–3
Disodium hydrogen phosphate (Na_2HPO_4)	7558–79–4
Deionized water	7732–18–5

potential to interact with the quartz surface. Specifically, additives with capabilities for polymer coating, metal chelation, and effects of commercial suppressants were selected because literature review and preliminary experiments indicated that these mechanisms might effectively reduce the generation of •OH radicals by quartz particles. The tested chemicals include octanohydroxamic acid (OHA), carboxy methyl cellulose (CMC), hydroxy propyl cellulose (HPC), poly(1-vinylpyrrolidone) (PVP), polyethylene glycol (PEG), and four commercial dust suppressants with assigned code names of CDS-A, CDS-B, CDS-C, and CDS-D. Details and the examined dosages of these chemicals are listed in Table 1. For each additive, two dosages were tested: a low dosage (D_1) and a high dosage (D_2). The initial dosage for each reagent was determined from both literature sources and preliminary trials, with careful consideration of occupational exposure limits based on the Workplace Environmental Exposure Levels (WEELs)™, as specified in the respective safety datasheets. These chemicals were primarily tested in DI water and the promising candidates for each dust sample were also evaluated in process water, tap water, and SLF.

2.3. Characterization

2.3.1. Particle size analysis

For particle size distributions (PSD) analysis of quartz dust samples, 0.1 g of the sample was first thoroughly mixed in a 10 mL glass beaker containing DI water, using a magnetic stirrer. A small portion of the resulting suspension was then transferred into the sample dispersion unit of a Malvern Panalytical Mastersizer 3000 laser diffraction analyzer using a micropipette. The dispersion unit was operated under controlled conditions to prevent particle settling and agglomeration. Three replicate measurements were performed to ensure reproducibility, and the average PSD was reported.

2.3.2. Elemental characterization

Inductively coupled plasma (ICP) mass spectroscopy was used to analyze the elemental compositions of the quartz samples and both tap water and process water. The SLF solution used in this study was obtained from Biochemazone™ (Alberta, Canada), with its composition listed in Table 2.

2.3.3. Surface area analysis

Surface area is a key surface chemistry property of respirable dust particles, significantly affecting their reactivity, oxidation rate, and interactions with lung tissues. For coal-quartz dust samples, the Brunauer–Emmett–Teller (BET) method using nitrogen gas as the adsorptive was used. The analysis was carried out over 125 min at a bath temperature of 77.35 K, with a relative pressure (p/p°) between 0.05 and 0.25. The absolute pressure ranged from 5.47 kPa to 24.39 kPa, while the adsorbed quantity varied between 0.05 mmol/g and 0.08 mmol/g at a saturation pressure of 97.78 kPa. Automatic degassing was utilized throughout the process.

2.3.4. Electrokinetic measurements

Zeta potential, which measures the effective electric surface charge, helps predict interactions between particles and reagents, as well as between particles themselves. This leads to various interfacial phenomena, such as reagent adsorption, film formation, and surface coating [48]. Particle zeta potential reveals the fundamental mechanisms behind various experimental observations. In this study, the zeta potentials of coal-quartz samples were measured across different solution pH levels. Details of the experimental procedure are provided in the supplementary material.

2.3.5. FTIR and XPS analysis

Fourier Transform Infrared (FTIR) spectroscopy using a Bruker® VERTEX 70 was utilized to analyze the surface functional groups of untreated and treated quartz dust particles. Randomly chosen dried quartz samples were used for this characterization. The IR spectra were recorded in the range of 4000–500 cm^{-1} with a resolution of 4 cm^{-1}. Each spectrum was obtained by averaging 32 scans to enhance the signal-to-noise ratio. The data were processed and evaluated using OPUS® spectroscopy software. Background spectra were collected and subtracted to correct for atmospheric interference and instrument noise. Pure gold was used as the reference for reflectance measurements to ensure accuracy and consistency. To minimize atmospheric interference, carbon dioxide gas was gently injected into the measurement chamber, purging the system. The instrument was cooled with liquid nitrogen to maintain optimal operating conditions, and the chamber was kept at a controlled temperature of 25 °C for stable measurements.

To determine and quantify the surface elemental compositions of both untreated and treated samples, x-ray photoelectron spectroscopy (XPS) analysis was performed. Before XPS analysis, the quartz powder samples were thoroughly rinsed with deionized water and left in a desiccator under partial vacuum for overnight soft drying. Detailed XPS procedures can be found in the supplementary material.

2.4. Fluorescence quantification of hydroxyl radicals

Fluorescence spectroscopy was utilized to measure •OH radicals released from the surface of quartz particles in aqueous solutions with varying qualities and pH. Terephthalic acid ($C_8H_6O_4$, >99 %), coumarin ($C_9H_6O_2$, >99 %), and coumarin-3-carboxylic acid (CCA, $C_{10}H_6O_4$, >99 %) were examined as chemical probes for •OH detection [49,50]. CCA proved to be the most effective chemical probe for detecting •OH across different pH levels in this study. In solution, CCA molecules react with •OH to form 7-hydroxycoumarin-3-carboxylic acid (7-OHCCA) [50]. This compound is a fluorescent molecule with a distinct emission peak at λ_{em} = 445nm. The fluorescence signal intensity is directly proportional to the concentration of 7-OHCCA and the amount of •OH

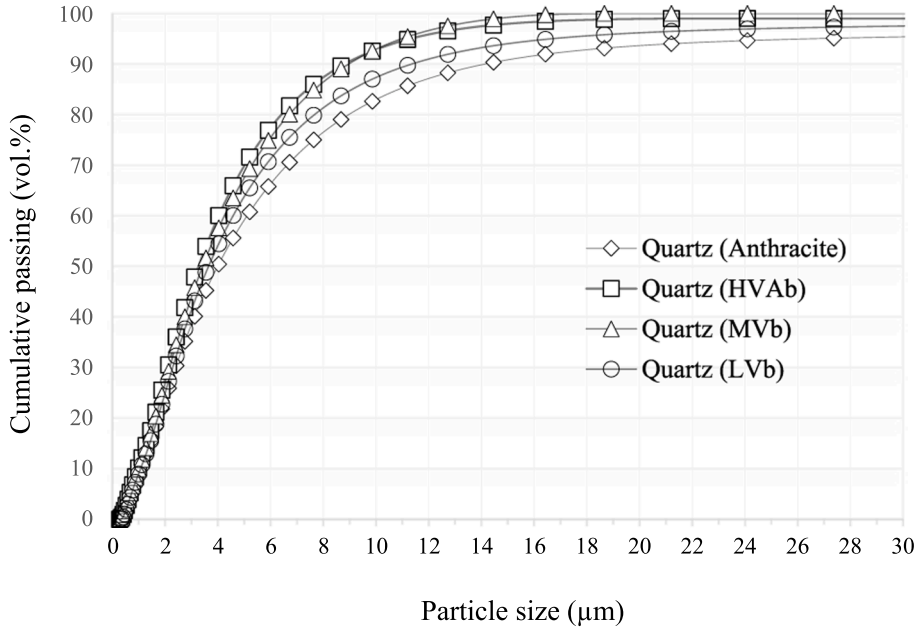

Fig. 1. Particle size distribution of the quartz dust samples.

present in the solution [50]. A calibration curve was created by preparing a series of standard 7-OHCCA solutions at different concentrations and transferring them into 3-mL standard polystyrene cuvettes. The fluorescence emission spectrum for each sample was recorded using a Shimadzu RF-6000 spectrofluorometer, with a scan speed of 200 nm/min, covering a wavelength range from 350 nm to 600 nm at 5 nm intervals, with an excitation wavelength of λ_{ex} = 387nm. The excitation and emission bandwidths were set to 3.0 nm and 1.0 nm, respectively, and all measurements were performed in the instrument's high-sensitivity mode. This spectrofluorometer is capable of detecting concentrations as low as $1 \times 10^{-1\ 3}$ mol/L with a signal-to-noise ratio of 1000:1 RMS (root mean square). The recorded intensity values were then plotted against the concentrations of the standard 7-OHCCA solutions in mol/L. A linear trend line was fitted to the data, establishing the relationship between fluorescence intensity and 7-OHCCA concentration, as shown in Fig. S-3. The detailed experimental procedure for •OH quantification is provided in the supplementary material.

2.5. Atomistic simulations

As the starting point for the atomistic simulations, a primitive cell of quartz was obtained from the Materials Project database, as shown in Fig. S-5-a [51]. The quartz primitive cell was fully relaxed (in terms of ion positions, cell size, and cell shape) using a cut-off energy of 400 eV and a *k*-points grid of 6 × 6 × 6. The fully-relaxed unit cell was then employed to generate a 2 × 2 × 1 slab, as shown in Fig. S-5-b. The obtained slab was then fully relaxed and was used to produce a (001) surface of quartz, since it is the most exposed, stable surface for the mineral [52]. The employed quartz structure has a trigonal crystal system in the space group P3_221, with lattice parameters of a = b = 4.92 Å and c = 5.43 Å with $\alpha = \beta = 90^{\circ}$ and $\gamma = 120^{\circ}$ [51, 53]. In the crystal structure of quartz, Si^{4+} is bonded to four equivalent O^{2-} atoms to form corner-sharing SiO_4 tetrahedra. There are two shorter (1.61 Å) and two longer (1.62 Å) Si-O bond lengths. Each O^{2-} atom is bonded in a bent geometry at 150 degrees to two equivalent Si^{4+} atoms [51]. Detailed protocols for DFT computations, AIMD simulations, and energy and charge calculations are provided in the supplementary material. All the *ab initio* computations and simulations were performed using the Vienna Ab initio Simulation Package (VASP) version 6.3 [54].

3. Results and discussion

3.1. Particle size, mineralogical, and elemental characterizations

The PSD results of the produced dust samples are shown in Fig. 1. As shown, the d_{80} of the obtained quartz dust samples is below 10 μm, the target particle size range for respirable dust. The XRD diffractograms are presented in Fig. 2, which confirmed the purity of the quartz samples. The elemental compositions of the quartz samples, and both tap water and process water are presented in Table 3 and Table 4, respectively. MVb quartz showed significantly higher levels of metal ions such as Fe, Al, Mg, K, Mn, Cu, Ni, Zn, and Cr compared to the other quartz samples. Process water had a higher concentration of Ca than tap water, while differences in other metal ion concentrations were present but minimal.

3.2. Effect of pH on •OH generation of quartz particles

Inhaled dust can alter the pH of biological fluids, significantly influencing particle-induced •OH formation as well as the dissolution and uptake of toxic dust constituents [55]. The impact of solution pH on •OH generation by coal-quartz particles was studied to understand how pH variations affect the reactivity and potential toxicity of the quartz samples. From Table 5, identical to all test cases, the generation of •OH on the bare quartz surface is more remarkable under the alkaline condition (pH 12) compared to the neutral and acidic conditions. The reason for this observation can be explained by the surface protonation of quartz at different solution pH conditions. In acidic conditions, high concentrations of H^+ ions lead to the formation of $Si\text{-}OH_2^+$, making the surface positively charged. At neutral pH, silanol groups primarily exist as Si-OH, rendering the surface relatively neutral. Conversely, in basic conditions, the abundance of OH^- ions results in the deprotonation of silanol groups to $Si\text{-}O^-$, giving the surface a negative charge [56, 57]. Further discussion on the effects of solution pH on surface charge, based on electrokinetic measurements, will follow in Section 3.4. The mechanical fracture of quartz crystals results in the breaking of Si–O–Si bonds, which connect the SiO_4 tetrahedra. This results in the formation of surface Si• and SiO• radicals [17]. By formulating the freshly cleaved (001) α-quartz surface hydroxylation in the presence of water molecules (Rxns. 1–3), it is seen that the availability of surface Si-O• radicals is

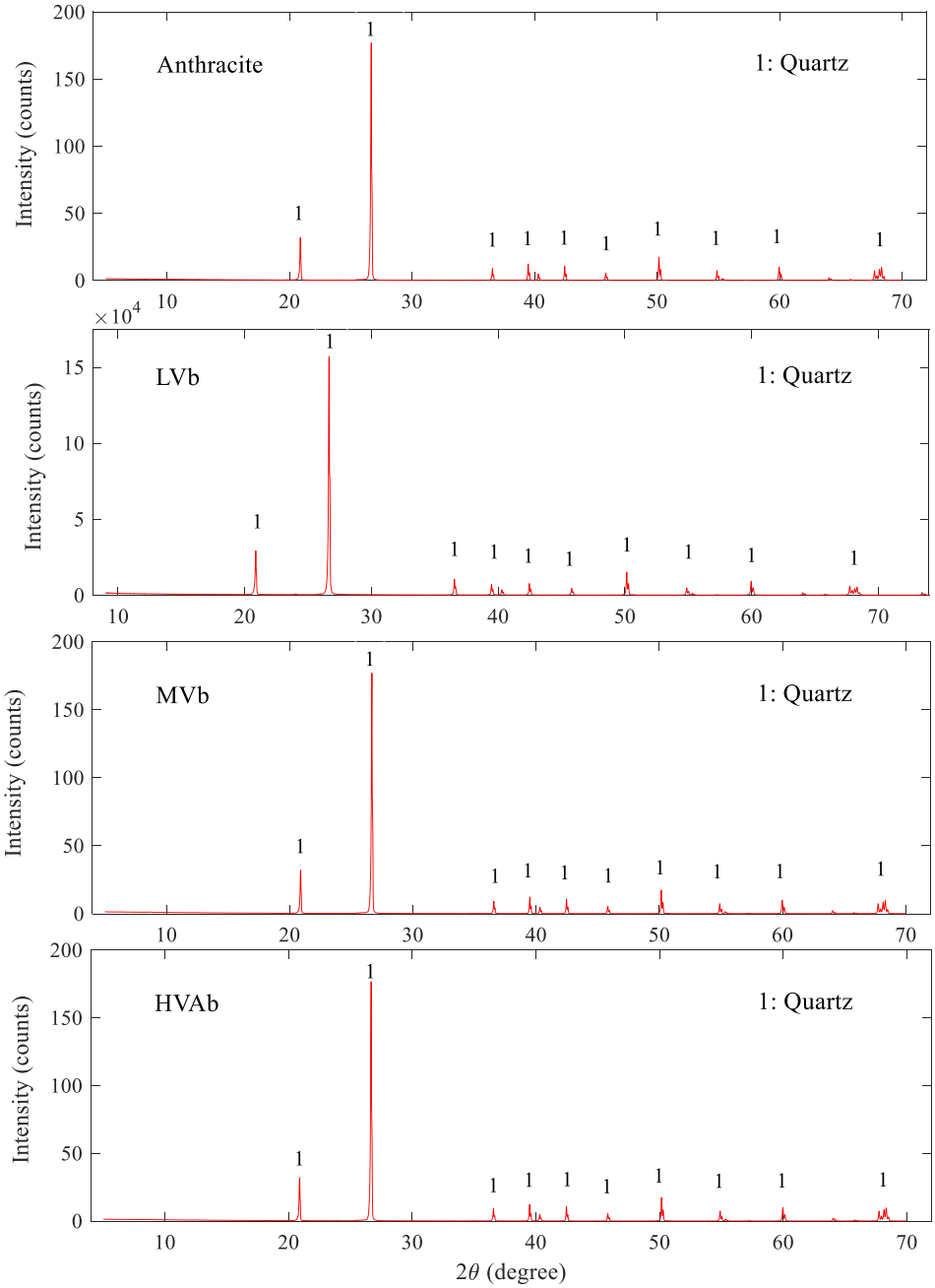

Fig. 2. X-ray powder diffractograms of Anthracite, LVb, MVb, and HVAb quartz samples.

favorable for the generation of silanol groups on the surface, which ultimately catalyzes the production of •OH and hydrogen peroxide [37].

$$\equiv SiO\bullet + H_2O \rightarrow \equiv SiOH + \bullet OH \quad (1)$$

$$\equiv SiO\bullet + \bullet OH \rightarrow \equiv SiOOH \quad (2)$$

$$\equiv SiOOH + H_2O \rightarrow \equiv SiO\bullet + H_2O_2 \quad (3)$$

3.3. Effect of chemical additives on •OH generation of quartz particles

The effects of various chemical additives were assessed on the •OH generation of anthracite, LVb, MVb, and HVAb coal-quartz samples under different solution pH conditions. The results for the various chemicals are presented in Table 5, where each recorded •OH concentration represents the average of three replicate tests. In the following sections, the impact of chemical treatment on the generation of •OH radicals on the surfaces of various quartz samples under different solution pH conditions are summarized, compared, and discussed.

OHA was tested at the two concentrations of 1.4×10^{-3} and 2.8×10^{-3} mol.L^{-1}. As shown in Table 5, in the case of the anthracite quartz, OHA exhibits a notable potential for the reduction of the quartz dust •OH generation at pH 12 at a concentration of 2.8×10^{-3} mol. L^{-1}; while it is not effective at neutral and acidic conditions. Moreover, the LVb, MVb, and HVAb quartz dust samples exhibit a higher •OH generation in aqueous media as compared to the anthracite quartz in their bare form. However, the OHA-treated LVb, MVb, and HVAb quartz samples exhibit a lower •OH generation compared to the anthracite quartz at the various solution pH. This could be explained by the possible presence of iron ($Fe^{2+/3+}$) as an impurity in the matrix of the LVb, MVb, and HVAb quartz samples, which can enhance the generation

Table 3
Concentration of main metal/ non-metal elements of the various quartz samples obtained from ICP-MS.

Element	Anthracite	LVb	MVb	HVAb
Fe	0.53 (wt%)	0.71 (wt%)	2.30 (wt%)	1.03 (wt%)
Al	0.16	0.20	0.40	0.16
Ca	807.00 (ppm)	578.00 (ppm)	773.00 (ppm)	734.00 (ppm)
Mg	50.00	59.00	323.00	53.00
Na	301.00	300.00	305.00	303.00
K	169.00	171.00	1001.00	144.00
Mn	14.00	15.00	113.00	17.00
Cu	4.00	7.00	30.00	11.00
Ni	13.00	16.00	77.00	26.00
Zn	20.00	20.00	30.00	22.00
P	93.00	92.00	89.00	91.00
Ti	109.00	111.00	141.00	106.00
Cr	322.00	348.00	1850.00	444.00

of •OH through a Fenton-like reaction, according to Rxn. 4 [60, 61].

$$Fe^{2+} + H_2O_2 \rightarrow Fe^{3+} + \bullet OH + OH^- \quad (4)$$

Contamination of the coal-quartz with trace levels of iron is possible due to the natural association of quartz with iron sulfides such as pyrite (FeS_2) in the coal deposits [60, 61]. Iron is the best-known transition metal capable of producing oxidants through Fenton, Haber-Weiss, or autoxidation reactions [62]. More discussion about the effects of iron will follow later in this study. On the freshly fractured (001) surface of α-quartz, the formation of siloxyl radicals leads to the generation of silanol groups and •OH when exposed to aqueous media (Rxns. 1 and 2) [37]. Such interactions lead to the production of hydrogen peroxide (H_2O_2) on the surface of quartz (Rxn. 3).

Hydroxamic acid (OHA) refers to a group of reagents capable of chelating with metallic atoms [63]. The adsorption of this reagent on mineral surfaces is known to be a frontier−orbital−controlled reaction, accompanied by charge transfer or covalent/coordination bond formation [64]. Considering the pK_a value of OHA at ~9.5 [65], at pH 12, OHA is present in its anionic form, while at pH 7 and 5 its protonated form is dominant. This can begin to explain the effective adsorption of OHA on the quartz surface at the alkaline condition, so that at pH 12 the anionic hydroxamate moiety chelates the surface silicon (Si) atoms preventing their role in the formation of surface silanol groups.

PEG was tested at the two concentrations of 1.95×10^{-4} and 3.9×10^{-4} mol.L^{-1}. As a hydrophilic polyether compound, PEG shows a notable potential for the reduction of quartz dust-induced •OH generation at the various solution pH (e.g., 85.2 % reduction at pH 7 on average), as shown in Table 5. The results indicate that PEG is effective at its initial dosage so that a higher dosage of the reagent does not offer a considerable benefit. Change in surface functional groups via coating seems to be the possible mechanism for the reduction of •OH on PEG-treated quartz surface [66]. The effectiveness of PEG is also enhanced as the solution shifts from acidic to neutral and then to basic conditions. PVP was tested at the two concentrations of 1.25×10^{-5} and 2.5×10^{-5} mol.L^{-1}. Comparing the results for the different quartz samples in Table 5, PVP brings about an average of 88.7 % reduction in the quartz •OH at pH 7. The higher dosage of PVP (2.5×10^{-5} mol. L^{-1}) did not offer a notable benefit at pH 7 and 12, except a slight improvement at pH 5. Like most of the tested chemicals, the effectiveness of PVP in reducing the quartz •OH favors the solution pH increase from acidic to neutral and basic. HPC was tested at the two concentrations of 0.62×10^{-5} and 1.24×10^{-5} mol.L^{-1}. HPC carries considerable potential in reducing the quartz •OH at the various pH conditions with an average reduction of 86.2 % at pH 7 at 0.62×10^{-5} mol. L^{-1}. The higher dosage of HPC (1.24×10^{-5} mol.L^{-1}) did not provide a remarkable benefit compared to its initial dosage. The performance of HPC also favors the solution pH elevation from acidic to neutral, and basic.

Commercial dust suppressants CDS-A and CDS-B were tested at the two dosages of 0.1 and 0.2 vol%. CDS-A, a synthesized blend of alkanes and alkylated organic compounds, offers a promising potential for the reduction of the quartz dust •OH at various solution pH especially at pH 7 and 12, as presented in Table 5. The optimum effective dosage for this chemical compound was found to be 0.2 vol%, at which CDS-A causes an average of 86.7 % reduction in the generation of •OH at pH 7. It is also evident that the effectiveness of this compound increases as the solution shifts from acidic to neutral and then to basic conditions. Treatment of quartz dust samples with CDS-B dust suppressant resulted in an average of 85.3 % reduction in their •OH at pH 7 at 0.1 vol% concentration. The effectiveness of the chemical compound enhances with an increase in solution pH.

Commercial dust suppressant CDS-C was tested at the two dosages of 1.0 and 2.0 vol%. The results in Table 5 indicate that this compound brings about a slight reduction in the quartz •OH at pH 5 and 7 using both 1 vol% and 2 vol% concentrations. A remarkable reduction in the generation of •OH is obvious under the alkaline condition especially at 2 vol% concentration. Moreover, this reagent offers a similar and better performance at pH 5 in the cases of the anthracite and HVAb quartz samples, compared to the LVb and MVb samples. However, a similarly better performance is evident at pH 7 in the cases of the anthracite, MVb, and HVAb quartz at 2 vol% concentration with an average of 83.64 % reduction in the •OH production.

Interestingly, as can be seen from Table 5 for CDS-A, -B, and -C commercial dust suppressants and PEG, the LVb quartz behaves differently in terms of inducing the production of •OH at pH 5 and 7 in its treated form compared to the three other quartz samples. This is not the case for the OHA-treated LVb quartz, which was discussed earlier. Such a discrepancy could be due to the presence of iron, which when treated with OHA, helps further reduce •OH generation through mediating the interaction of OHA molecules with the mineral surface (as a metal chelator). Otherwise, iron contributes to the enhanced •OH generation of the LVb quartz (Rxn. 4). Such an observation reveals that the presence of a metal-chelating ingredient in the composition of the chemical candidates does play an important role in their capability to suppress the contribution of iron to the •OH generation of the quartz.

Commercial dust suppressant CDS-D was also tested at the two dosages of 0.15 and 0.30 vol%. The results in Table 5 indicate that this compound does not show an effective performance at pH 5 and 7, while at pH 12 a remarkable reduction in •OH content is evident. This chemical compound offers an average of 65.5 % reduction in the •OH of the various quartz samples at pH 7. Moreover, comparing the results corresponding to the quartz samples treated with CDS-D at various solution pH, it is seen that moving from the anthracite quartz towards the LVb, MVb, and HVAb quartz, the effectiveness of the reagent drops significantly at pH 7 as well as for most cases at pH 5. The optimum effective concentration for this chemical compound was found to be 0.15 vol%. It is also worth noting that for the commercial dust suppressants evaluated in this study, no information is available with regards to their chemical composition, molecular weight, density, etc. Therefore, we were not able to further elaborate on the mechanisms of

Table 4
Concentration of main metal/ metalloid elements of the tap water and process water samples obtained from ICP-MS.

Water	Distribution of main elements (ppm)								
	Fe	Ca	Mg	B	K	Sr	Cu	Si	Zn
Process	0.08	259.10	14.40	2.00	12.20	4.00	0.00	6.00	0.00
Tap	0.02	36.80	16.00	0.80	1.00	0.00	0.25	3.00	0.30

Table 5
Chemical additive test matrix for the quartz samples associated with coals of various ranks.

Quartz	pH	Hydroxyl radical concentration (10^{-9} mol.L^{-1}, ± 95 % CI)																	
		Bare	OHA		PEG		PVP		HPC		CMC		CDS-A		CDS-B		CDS-C		CDS-D	
			D_1	D_2	D_1	D_2	D_1	D_2	D_1	D_2	D_1	D_2	D_1	D_2	D_1	D_2	D_1	D_2	D_1	D_2
Anthracite	5	48.5 ± 5.2	45.0 ± 4.7	33.9 ± 3.5	16.4 ± 2.9	17.0 ± 3.5	20.2 ± 2.9	17.8 ± 3.2	25.0 ± 3.4	16.2 ± 2.9	6.6 ± 1.9	5.8 ± 2.2	20.6 ± 2.9	17.8 ± 3.4	20.6 ± 3.2	16.4 ± 3.4	31.5 ± 6.4	33.9 ± 5.9	28.4 ± 3.7	15.8 ± 2.4
	7	65.4 ± 6.7	63.3 ± 6.7	58.7 ± 5.7	10.3 ± 1.7	9.1 ± 1.5	8.2 ± 2.2	8.2 ± 2.4	13.2 ± 3.4	9.8 ± 2.7	6.2 ± 1.9	6.2 ± 1.7	10.6 ± 4.7	9.0 ± 3.4	7.9 ± 2.2	6.2 ± 1.9	23.6 ± 4.7	15.2 ± 3.4	12.2 ± 4.2	12.0 ± 4.4
	12	1562.0 ± 47.2	121.0 ± 29.8	26.0 ± 3.9	20.6 ± 4.4	9.1 ± 1.7	4.8 ± 1.2	4.4 ± 1.5	5.0 ± 1.9	4.4 ± 2.2	9.2 ± 2.7	9.0 ± 2.4	4.7 ± 1.9	4.2 ± 2.2	4.0 ± 1.4	5.2 ± 1.9	41.2 ± 8.4	21.2 ± 4.9	4.2 ± 1.7	4.0 ± 2.2
LVb	5	56.6 ± 5.9	28.6 ± 3.7	23.2 ± 3.4	32.8 ± 5.7	25.4 ± 4.5	29.8 ± 4.4	22.6 ± 3.7	32.6 ± 4.7	22.6 ± 5.2	7.2 ± 1.9	6.8 ± 2.2	37.2 ± 5.5	28.6 ± 4.7	36.2 ± 4.2	27.4 ± 3.4	52.6 ± 9.4	48.6 ± 8.6	38.6 ± 6.7	29.6 ± 4.4
	7	74.8 ± 9.2	14.0 ± 2.7	12.0 ± 2.5	19.8 ± 4.2	13.6 ± 2.7	10.2 ± 1.9	9.0 ± 2.7	14.2 ± 3.4	13.2 ± 3.9	6.8 ± 1.9	5.8 ± 1.9	21.4 ± 3.9	14.8 ± 2.7	20.8 ± 4.4	15.4 ± 3.2	60.2 ± 10.4	55.4 ± 9.6	17.4 ± 3.2	16.2 ± 4.7
	12	1588.0 ± 44.7	92.3 ± 14.4	10.2 ± 3.2	9.4 ± 1.2	4.2 ± 1.5	9.4 ± 2.2	9.4 ± 1.9	9.6 ± 2.5	9.0 ± 2.9	9.2 ± 2.4	9.2 ± 2.2	10.2 ± 3.2	4.6 ± 2.2	11.2 ± 2.4	3.8 ± 1.4	102.8 ± 13.1	15.2 ± 4.7	19.0 ± 2.9	10.8 ± 1.9
MVb	5	64.4 ± 5.9	21.3 ± 3.4	14.1 ± 2.2	19.2 ± 4.2	15.0 ± 3.2	18.9 ± 3.9	16.5 ± 2.9	21.9 ± 4.5	18.9 ± 5.2	6.4 ± 1.7	6.2 ± 1.9	24.9 ± 4.4	19.2 ± 5.2	18.6 ± 5.2	16.2 ± 3.2	63.9 ± 10.7	38.1 ± 7.1	37.6 ± 6.2	31.1 ± 6.9
	7	96.6 ± 8.9	7.2 ± 2.0	6.3 ± 1.7	8.1 ± 2.2	6.9 ± 1.2	9.3 ± 1.9	7.2 ± 1.9	7.9 ± 2.2	6.8 ± 1.2	7.0 ± 1.9	6.6 ± 2.2	8.1 ± 1.7	7.2 ± 2.2	8.1 ± 2.2	7.5 ± 1.9	14.1 ± 2.9	13.2 ± 2.7	42.0 ± 9.1	40.8 ± 7.9
	12	1682.0 ± 57.1	65.1 ± 10.7	13.8 ± 2.9	14.1 ± 2.9	14.1 ± 2.7	15.6 ± 2.9	12.6 ± 3.4	14.7 ± 4.2	14.4 ± 3.2	9.6 ± 2.7	9.6 ± 2.4	13.8 ± 2.9	13.5 ± 4.2	13.8 ± 2.9	14.1 ± 4.2	15.3 ± 2.2	15.6 ± 2.7	15.0 ± 2.9	15.0 ± 2.7
HVAb	5	59.8 ± 7.7	20.0 ± 4.0	18.8 ± 4.2	15.2 ± 3.4	13.2 ± 2.2	17.0 ± 4.7	14.2 ± 3.2	21.4 ± 4.5	18.6 ± 3.2	7.8 ± 2.9	6.8 ± 2.2	33.2 ± 7.6	22.0 ± 4.2	25.8 ± 4.9	21.0 ± 3.7	42.2 ± 6.4	27.0 ± 4.4	36.8 ± 7.2	34.2 ± 6.4
	7	89.5 ± 10.4	8.6 ± 2.2	7.4 ± 1.9	7.8 ± 1.4	7.5 ± 1.5	8.3 ± 2.2	7.5 ± 2.7	7.1 ± 2.7	6.0 ± 2.9	10.0 ± 2.9	7.0 ± 2.7	12.5 ± 3.7	10.8 ± 3.2	9.5 ± 2.7	8.7 ± 2.4	11.5 ± 2.4	10.9 ± 2.9	47.0 ± 7.6	44.2 ± 7.4
	12	1625.0 ± 52.1	74.2 ± 12.9	17.6 ± 3.9	9.2 ± 1.7	9.2 ± 1.4	8.6 ± 1.9	8.2 ± 1.7	9.2 ± 2.2	8.4 ± 2.4	10.4 ± 3.2	9.2 ± 3.2	9.6 ± 2.7	9.6 ± 2.2	10.9 ± 2.2	8.6 ± 1.7	20.6 ± 3.4	13.6 ± 3.9	10.2 ± 2.4	10.2 ± 2.4

Table 6
Effect of aqueous solution quality and composition on the quartz •OH in bare and CMC/OHA-treated forms; pH 7–8.

Quartz	•OH concentration (10^{-9} mol. L^{-1}, ± 95 % CI)											
	DW			TW			PW			SLF		
	Bare	CMC	OHA	Bare	CMC	OHA	Bare	CMC	OHA	Bare	CMC	OHA
Anth.	65.4 ± 6.7	6.2 ± 2.0	58.7 ± 5.7	54.4 ± 8.9	4.6 ± 2.5	32.0 ± 2.8	18.0 ± 5.4	8.8 ± 2.2	11.8 ± 2.2	16.6 ± 4.7	5.8 ± 1.7	7.0 ± 2.7
LVb	74.8 ± 9.2	6.8 ± 1.9	12.0 ± 2.5	58.7 ± 10.4	6.1 ± 2.0	12.0 ± 1.9	19.2 ± 6.7	8.2 ± 2.7	10.0 ± 2.7	16.2 ± 3.4	5.3 ± 2.5	6.2 ± 2.4
MVb	96.6 ± 8.9	7.0 ± 1.8	6.3 ± 1.7	67.8 ± 9.7	8.6 ± 3.0	9.8 ± 1.5	25.4 ± 5.9	8.4 ± 2.7	8.2 ± 2.2	18.4 ± 4.7	5.8 ± 2.2	7.2 ± 2.4
HVAb	89.5 ± 10.4	10.0 ± 2.9	7.4 ± 1.9	69.2 ± 10.2	9.2 ± 2.4	7.8 ± 0.9	24.1 ± 7.7	9.8 ± 2.4	8.8 ± 2.7	16.8 ± 2.9	8.8 ± 2.2	8.8 ± 3.2

interactions of these chemical reagents with the mineral dust surface.

In the current research, the potential of CMC (used as its sodium salt) was also evaluated as a chemical additive to reduce/inhibit the quartz dust •OH. CMC was evaluated at the two concentrations of 0.76×10^{-3} and 1.52×10^{-3} mol.L^{-1}. The results in Table 5 indicate that CMC is remarkably effective in inhibiting the quartz •OH at various pH conditions. At pH 7, the quartz •OH is reduced by ~91 % when treated with 0.76×10^{-3} mol.L^{-1} of CMC. CMC exhibits a consistent effectiveness at the various solution acidity so that the elevation of pH does not notably affect its performance in reducing the quartz •OH. Compared to the other chemical additives examined in the current research, CMC showed the highest effectiveness in inhibiting the quartz dust •OH. Also, CMC is effective on all the four different coal-quartz samples investigated in the current study. This indicates that the possible difference between the various quartz samples with regards to the trace-level presence of certain metal ions, such as $Fe^{2+/3+}$ in their matrix, does not influence the capability of CMC in suppressing the •OH generation.

Based on the elemental compositions of the different quartz samples in Table 3, MVb quartz contains significantly higher amounts of certain metal ions in comparison to the other quartz samples. This is in conformity with the highest •OH generation induced by MVb quartz at various solution pH in comparison to the other quartz samples. This confirms the importance of certain metal ions (present as impurity) in the generation of •OH by quartz dust.

To summarize, the results in Table 5 demonstrate that •OH generation of coal-quartz samples is influenced by both their composition, particularly the presence of metals like iron, and the solution pH. The study identified key chemical additives, such as CMC, that effectively inhibit quartz •OH generation and potentially reduce its toxicity across all samples and pH levels. Some commercial dust suppressants were also effective in reducing •OH generation, especially under alkaline conditions, though performance varied across different quartz samples.

Different aqueous solutions, i.e., tap water (TW, pH 7.8), process water (PW, pH 8), and SLF (pH 7.4) were also evaluated for the quartz samples in their bare form and treated with CMC (0.76×10^{-3} mol.L^{-1}) and OHA (2.8×10^{-3} mol. L^{-1}) using the fluorescence values for •OH. The results were compared with those obtained using DI water (DW) to investigate how the quality and composition of aqueous media affect the surface-coating capability of CMC and metal-chelating capability of the hydroxamic acid on the quartz surface. As shown in Table 6, for all quartz samples, the generation of •OH in various aqueous media followed the sequence: DW > TW > PW > SLF. The varying quality and composition of the aqueous media did not remarkably affect the effectiveness of CMC in reducing the quartz dust •OH.

The results indicate that the varying quality and composition of the aqueous media remarkably affects the effectiveness of OHA in reducing the anthracite quartz dust •OH. However, in the cases of the LVb, MVb, and HVAb quartz samples, the varying solution quality and composition do not notably affect the quartz−OHA interaction while slight differences are evident. This might be because the iron in the matrix of these quartz samples outcompetes the other metal ions present in TW, PW, and SLF solutions in mediating the OHA−quartz interaction through activating the quartz surface (i.e., being a more favorable hydrolyzed metal ion to adsorb on the quartz surface) [63, 67]. In other words, this can also be explained by the possible higher affinity of OHA for $Fe^{2+/3+}$ ions in solution as compared to the other metal ions. Moreover, the •OH inhibiting capability of OHA on the quartz surface is improved for the cases of the LVb, MVb, and HVAb quartz as opposed to anthracite quartz in tap water as well as in DI water. The capability of OHA does not vary significantly in the process water and SLF when comparing the corresponding cases of the four different quartz samples.

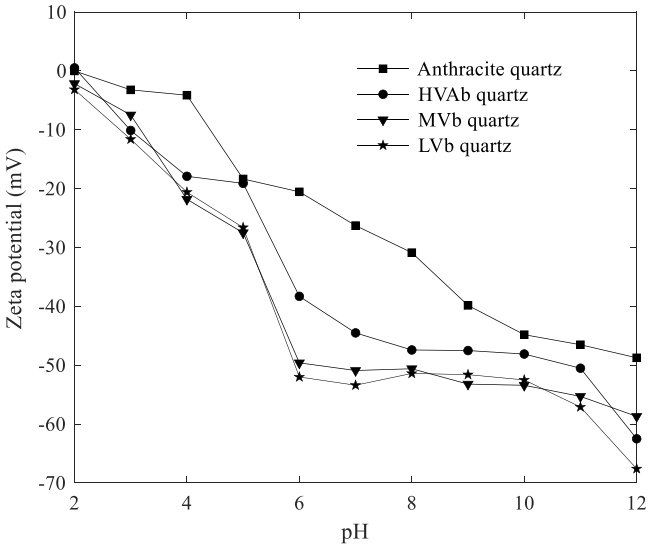

Fig. 3. Zeta potential of the quartz samples as a function of solution pH (STD < 2 mV).

3.4. Surface characterization

3.4.1. Surface area analysis

The BET results were identical for the different coal-quartz dust samples, indicating a specific surface area of 4.5 m^2/g with a pore size and volume of 11.8 Å and 0.001 cm^3 /g, respectively.

3.4.2. Electrokinetic measurements

The variation in zeta potential with solution pH for different coal-quartz samples in DI water is illustrated in Fig. 3. The isoelectric point (IEP) for quartz is observed around pH 2, indicating that quartz surfaces are typically negatively charged in biological environments (pH 7.4), which may contribute to disease development [56, 68]. In an aqueous environment, the Si• and SiO• radicals on the freshly fractured quartz surface tend to form silanol groups [69]. The silanol groups, due to their Brønsted acidity, play a crucial role in the quartz surface charge development by either accepting or donating protons (H^+ ions) depending on the pH of the surrounding medium [56]. At low pH, silanol groups tend to accept protons, leaving the quartz surface with a positive charge ($SiOH_2^+$). At alkaline pH, silanol groups donate protons, resulting in a negatively charged surface (SiO^-) [57].

The point zeta potentials were measured for the quartz samples in the different aqueous solutions (TW, PW, and SLF). The point measurements were conducted at the original pH of the solutions with no pH

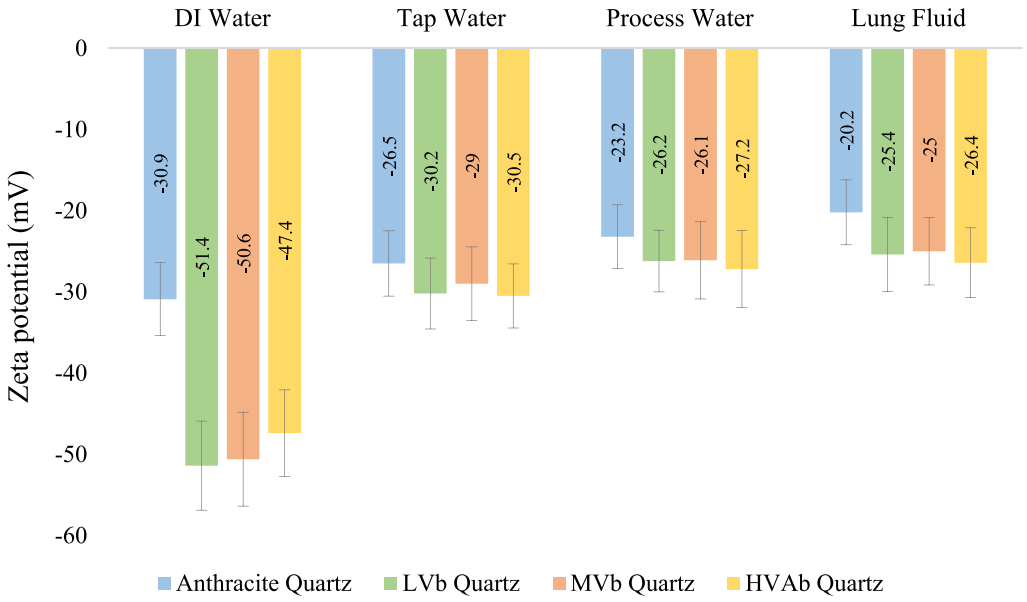

Fig. 4. Zeta potentials of various quartz samples in different aqueous solutions with original pH of 7–8. Error bars indicate 95 % confidence interval.

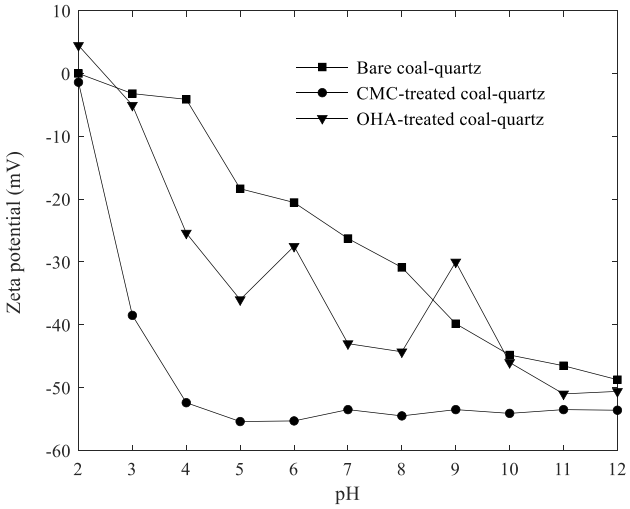

Fig. 5. Zeta potentials of bare and CMC- and OHA-treated anthracite quartz samples as a function of solution pH (CMC: 0.76 $\times 10^{-3}$ mol.L^{-1}, OHA: 2.8 $\times 10^{-3}$ mol.L^{-1}).

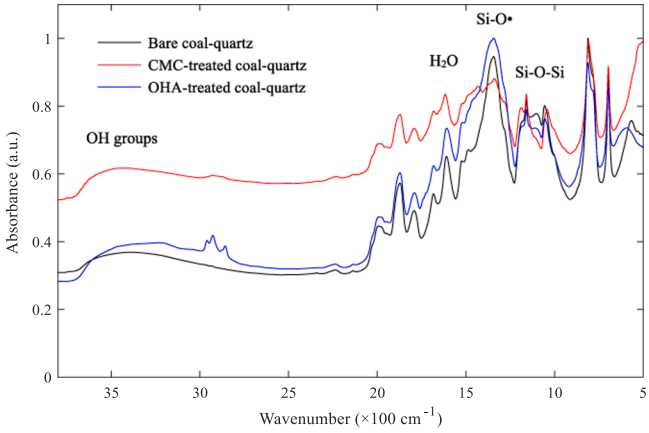

Fig. 6. IR spectrum of the bare and CMC/ OHA -treated anthracite quartz samples (CMC: 0.76 $\times 10^{-3}$ mol.L^{-1}, OHA: 2.8 $\times 10^{-3}$ mol.L^{-1}).

adjustment (see Fig. 4; error bars indicate 95 % confidence interval). These values were compared with the results using DI water at pH ~7.6. For all quartz samples, the surface charge negativity, as indicated by zeta potential values, decreases in the sequence: DW > TW > PW > SLF. Among the tested quartz samples, anthracite quartz showed the least negative surface charge compared to the other quartz samples, which showed a similar surface charge in the different solutions. Comparing these results with the corresponding •OH values in Table 6, it can be inferred that there is a direct relationship between the negativity of the quartz surface charge, and its potential for generation of •OH. In other words, a more negative quartz surface allows production of more •OH, under the conditions of the current study. From Table 6, quartz-induced •OH in TW is higher than in PW. This might be due to the higher Ca content of PW compared to TW, which may help mask the quartz surface siloxyl radicals leading to a less negative quartz surface and, therefore, a reduced generation of •OH.

Additionally, zeta potential measurements were performed for anthracite quartz samples treated with CMC (0.76 $\times 10^{-3}$ mol.L^{-1}) and OHA (2.8 $\times 10^{-3}$ mol.L^{-1}) as a function of solution pH, and the results compared with those for the bare quartz particles in Fig. 5. The adsorption of CMC on the quartz surface shifts the zeta potentials of quartz towards significantly more negative values compared to the bare mineral. From pH around 5 to pH 12, the zeta potential of CMC-treated quartz remains a constant negative value, which may indicate that the effective adsorption of CMC on the quartz surface takes place at the pH range of 2–5. The adsorption of CMC on the hydroxylated (001) α-quartz surface may occur through the mediation (bridging) of certain metal ions in the system, e.g., Na^{+}, $Fe^{2/3+}$, and Ca^{2+}, between the COO^{-} moieties of CMC and the quartz surface. Except at pH 2 and pH 9, the adsorption of OHA on the quartz surface results in a slightly more negative zeta potential over the range in pH compared to the bare mineral. The sharp change in the behavior of OHA on the quartz surface at pH ~9 could be due to the pK_a of this reagent occurring at ~9.5.

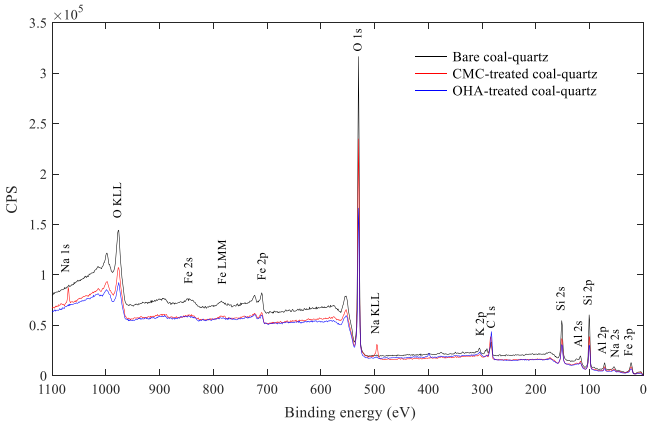

Fig. 7. XPS survey spectrums of the bare and CMC-treated quartz samples (CMC: 0.76 $\times 10^{-3}$ mol.L^{-1}, OHA: 2.8 $\times 10^{-3}$ mol.L^{-1}).

3.4.3. FTIR analysis

To further understand the behavior of the quartz surfaces with CMC and OHA reagents, FTIR spectra were obtained for selected quartz samples. The IR spectra for the freshly ground bare, OHA- and CMC-treated anthracite quartz samples are presented in Fig. 6. On the bare quartz surface, the sharp IR band at 1340 cm^{-1} is characteristic of Si-O•. Comparing this band for the bare and treated samples, it is evident that because of treatment by CMC, the Si-O• sites are masked on the quartz surface. This is in line with the results of the •OH quantification experiments for CMC-treated quartz samples; the amount of •OH diffused by the quartz dust at various solution pH is reduced, e.g., by ~91 % at pH 7 [70]. The adsorption of OHA and CMC (organic compounds) on the surface of the quartz dust is further supported by the appearance of two new IR absorption peaks between 2840 cm^{-1} and 3000 cm^{-1}. These two peaks could be assigned to the -C-H stretching [70].

3.4.4. XPS analysis

The surface compositions of the selected quartz samples were determined using the XPS technique before and after treatment with CMC and OHA reagents. Survey spectra, and atomic concentrations of various elements/species on the quartz surfaces are found in Fig. 7 and Table 7, respectively. The survey spectra show the major characteristic peaks of the elements present on the bare and treated quartz surfaces. The CMC-treated quartz surface is higher in organic species, e.g., C-O, C═O, and CH_x, compared to the bare mineral, as shown in the high-resolution C1s spectra presented in Fig. 8. On the OHA-treated surface, there is a remarkable increase in the concentrations of CH_x and C═O, while the concentrations of C-O and COO remain unchanged compared to the bare quartz surface, as shown in Table 7 and Fig. 8. The presence of Fe and Al ions on the bare quartz surface is evident from the survey spectra shown in Fig. 7, which corroborates the surface atomic compositions listed in Table 7. The amount of Fe and FeO_x species on the quartz surface decreases following CMC and OHA treatments, as detailed in Table 7 and depicted in Fig. 9, respectively. Similarly, the concentrations of other metal ions, including Si and Al, decrease on the quartz surface due to these treatments.

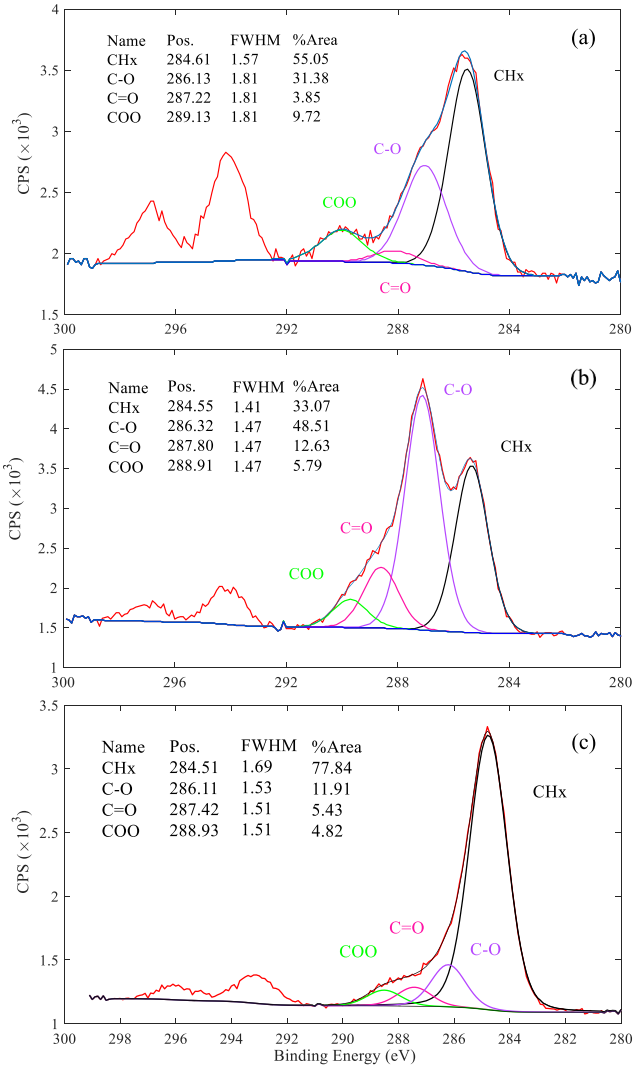

Fig. 8. C1s spectra for (a): bare, (b): CMC-treated, and (c): OHA-treated quartz samples (CMC: 0.76 $\times 10^{-3}$ mol.L^{-1}, OHA: 2.8 $\times 10^{-3}$ mol.L^{-1}).

3.5. Effect of surface aging on •OH generation by quartz particles

Freshly generated coal-quartz dust samples were spread as a thin layer on a clean, flat surface and left in open air at room temperature for eight hours in a laboratory environment to obtain the aged samples. The aged samples were evaluated for their •OH generation in DI water at pH 7. The results are presented in Fig. 10 (error bars indicate 95 % confidence interval), which show that the atmospheric surface aging results in a slight decrease in the •OH generation of the quartz particles. This agrees with various experimental studies in which freshly ground mineral quartz samples have shown a higher degree of toxicity than the aged quartz samples [58, 71, 72]. The reason for this is that the availability of surface siloxyl radicals on the surface of freshly cleaved quartz is essential for the generation of silanol groups and ultimately •OH in aqueous media [37]. However, studies involving electron paramagnetic resonance (ESR) spectroscopy have shown that siloxyl radicals on the

Table 7
Concentration of elements and species on the surface of bare and treated coal-quartz samples (at%), CMC: 0.76 × 10^{-3} mol.L^{-1}, OHA: 2.8 × 10^{-3} mol.L^{-1}.

Quartz	C_T	CH_x	C-O	C═O	COO	Al	Fe	K	Na	O	Si
Bare	8.5	4.7	2.7	0.3	0.8	4.5	1.3	0.8	-	59	26
CMC-treated	19.8	6.5	9.6	2.5	1.1	3.7	0.9	0.5	2	52	21
OHA-treated	24.3	19.3	2.7	1.2	1.0	3.7	0.7	0.7	-	47.1	21.6

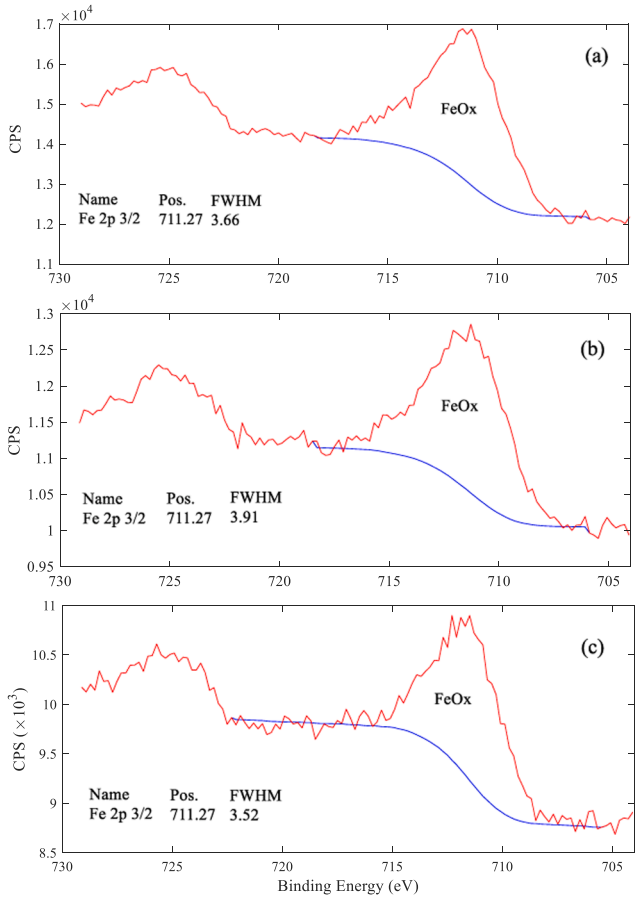

Fig. 9. Comparison of Fe 2p spectra for (a): bare, (b): CMC-treated, and (c): OHA-treated quartz samples (CMC: 0.76 $\times 10^{-3}$ mol.L^{-1}, OHA: 2.8 $\times 10^{-3}$ mol.L^{-1}).

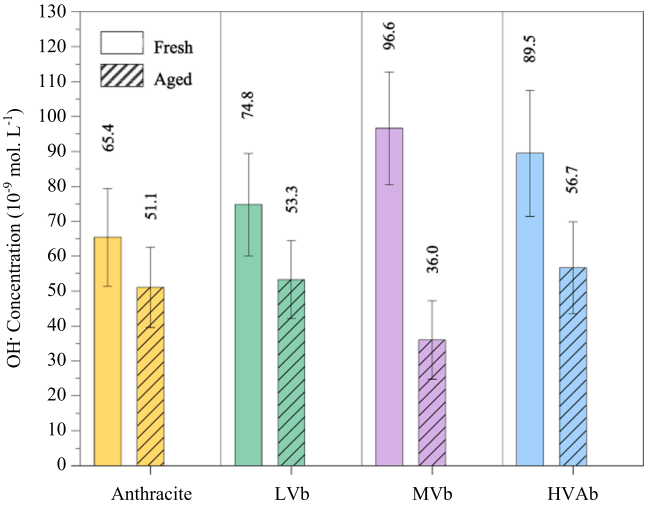

Fig. 10. Effect of surface aging on the generation of •OH by the coal-quartz dust samples associated with coals of various ranks. Error bars indicate 95 % confidence interval.

freshly cleaved quartz surface decay as function of time on exposure to the atmosphere, with a half-life of about 36 h [73, 74]. The presence of water (moisture) may accelerate this decay process [38]. In experimental *in vivo* studies, freshly ground silicas have shown a higher degree of toxicity than aged ones [75, 76]. Fig. 11 compares the IR spectra for

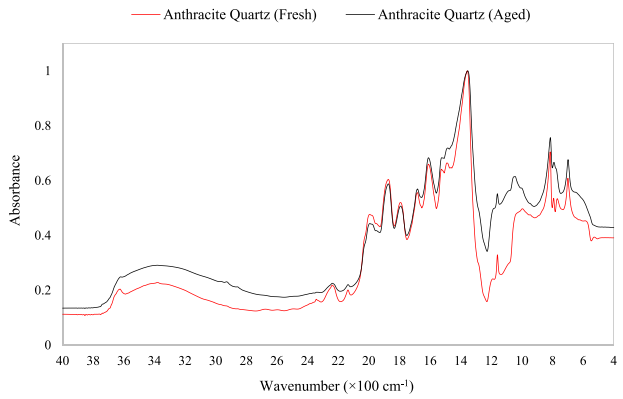

Fig. 11. IR spectrum for freshly ground and aged anthracite quartz samples.

both freshly ground and aged anthracite quartz samples, in which the disappearance of the -OH characteristic peak at 3622 cm^{-1} on the surface of aged quartz is evident.

3.6. Atomistic simulations

The results in Table 5 indicate that quartz samples with higher iron contamination (LVb, MVb, and HVAb) exhibit greater •OH production. Interestingly, when treated with OHA at pH 7, •OH production of these quartz samples is reduced by an average of 89.7 %, compared to a 10.3 % reduction for anthracite quartz, which has the lowest iron content. To better explain this contrasting effect of iron, we further investigated quartz surface interactions in the presence of iron using AIMD simulations. First, the adsorption configuration of iron-hydroxide on the quartz surface was simulated, followed by exposure of the iron-treated surface to an oxygen molecule. The results of these simulations are presented in Fig. 12. The adsorption energies calculated for various interaction configurations are detailed in Table 8. Fig. 12-a shows that iron in the form of $Fe(OH)_3$ molecule adsorbs onto the hydroxylated quartz (001) surface through the formation of a bond between the iron atom and an oxygen atom on the surface. The energy associated with this adsorption is −380 kJ·mol^{-1}, and the bond length is measured at 2.0 Å. In the presence of molecular oxygen (Fig. 12-b), the iron-treated quartz surface leads to the formation of H_2O_2 with an energy of −264 kJ·mol^{-1}, and results in a deprotonated iron-treated surface, as shown in Fig. 12-c. The produced H_2O_2 can dissociate into •OH and hydroxide ion (OH^-) in the presence of ferrous iron, following Rxn. 4 [58,59]. This explains the enhanced generation of •OH by the coal-quartz including HVAb and MVb samples with higher content of iron impurity.

To investigate whether the presence of iron influences the adsorption of the hydroxamic acid molecule on the quartz surface, we compared the adsorption energy and configuration of OHA on the bare quartz surface with those on the iron-treated surface, as shown in Fig. 13 and Table 8. On the bare quartz surface, OHA molecule adsorbs by establishing a tridentate bond between a sodium cation and the two oxygen atoms and one nitrogen atom of the hydroxamate group (Fig. 13-a). The bridging sodium ion is adsorbed on two oxygen atoms of the quartz surface, without substituting the corresponding surface protons. Through a similar configuration, OHA molecule adsorbs on the two oxygen atoms of the iron-treated quartz surface (Fig. 13-b). Comparing the adsorption energies in Table 8, it is evident that the OHA molecule establishes stronger and more favorable adsorption on the iron-treated (001) quartz surface compared to the bare mineral surface. This could be explained by the chelating affinity of hydroxamic acids towards the metallic ions [77, 78]. A Fe-mediated surface coating of quartz particles by OHA molecules would not only neutralize the role of $Fe^{2+/3+}$ itself but also help prevent the formation of surface silanol groups via a stronger coverage of quartz surface by the OHA molecules.

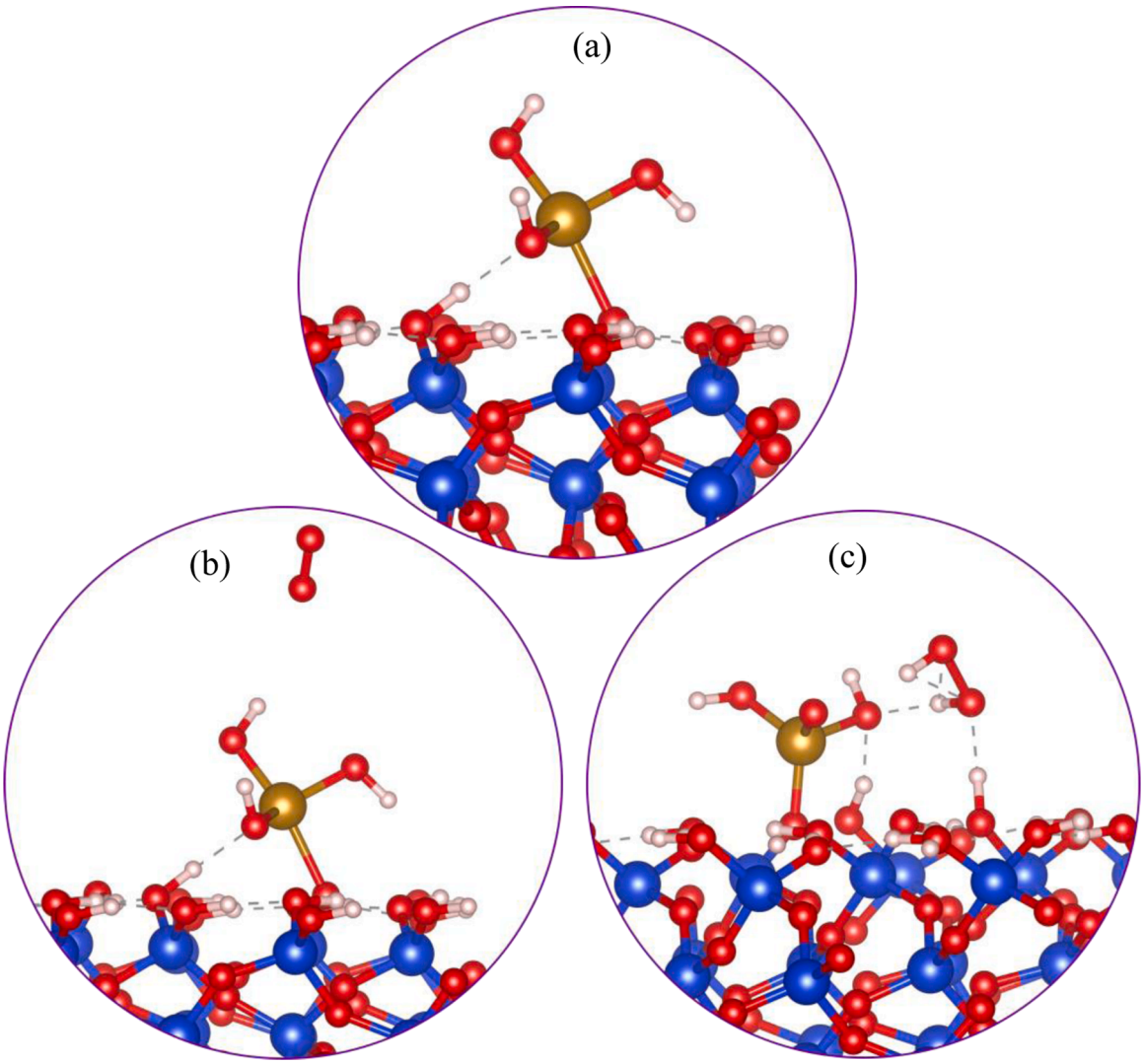

Fig. 12. Adsorption configurations of iron-hydroxide on the (001) quartz surface, and the interaction of oxygen molecule with the iron-treated quartz surface.

Table 8
Adsorption energies for interactions of iron hydroxide, molecular oxygen, and OHA on the quartz (001) surface.

Molecule	Substrate	Ads. Energy (kJ.mol^{-1})
$Fe(OH)_3$	(001) quartz	−380
O_2	Fe-treated (001) quartz	−264
OHA	(001) quartz	−75
OHA	Fe-treated (001) quartz	−117

The insights into chemical interactions and additive combinations identified in this study have practical implications for coal mining operations. Specifically, these findings can be applied to enhance the efficiency of dust-suppressing water sprays and improve the performance of conventional dust control devices such as Brattice cloth and dust filters. Moreover, this research opens up the possibility of developing tailored additive formulations that target specific coal components, thereby reducing dust toxicity and associated health risks. Future pilot-scale studies in operational settings are planned to validate these measures and facilitate their practical implementation in the coal mining industry and beyond.

4. Conclusions

Prolonged exposure to quartz dust can cause severe respiratory diseases. In this study, quartz samples associated with coals of various ranks were evaluated for hydroxyl radical generation in different aqueous solutions across different pH levels. The fluorescence values were used as a measure to quantify •OH concentrations. Safe chemical additives were evaluated for their ability to inhibit •OH generation of the quartz. This study offers several key insights:

- Fresh quartz surfaces favor the generation of •OH, particularly in alkaline conditions.
- CMC in its sodium salt form significantly inhibits this •OH generation across various pH levels, achieving about a 91 % reduction at pH 7.
- The generation of •OH in quartz is least observed in lung fluid (17 $\pm$ 3.9 10^{-9} mol. L^{-1} on average), followed by process water (21.7 $\pm$ 6.5 10^{-9} mol. L^{-1}), tap water (62.5 $\pm$ 9.8 10^{-9} mol. L^{-1}), and DI water (81.6 $\pm$ 8.9 10^{-9} mol. L^{-1}).
- The negative charge on the quartz surface in different aqueous solutions is directly linked to •OH generation, with the order being DI water, tap water, process water, and lung fluid.
- In all tested media, anthracite quartz exhibits the least negative surface charge, contrasting with other quartz types.
- The exposure of coal-quartz samples to ambient air results in a slight decrease in •OH generation over time due to the decay of surface siloxyl radicals.

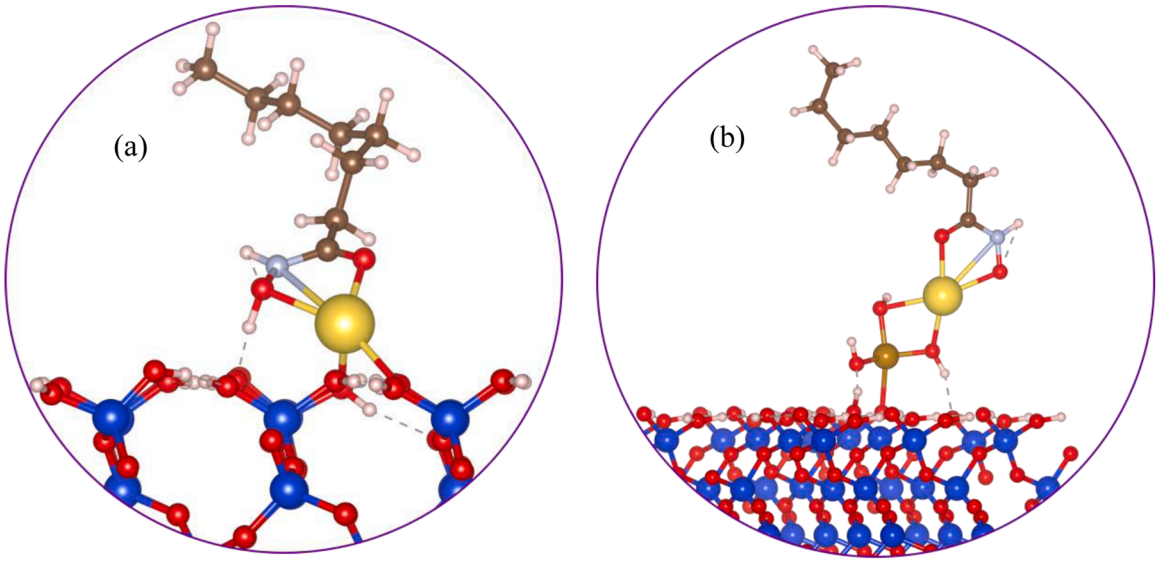

Fig. 13. Adsorption configurations of OHA on the bare as well as on the iron-treated (001) quartz surface.

- Atomistic simulations confirm that iron catalyzes the production of hydrogen peroxide, an essential reactant for •OH production, on the quartz surface in the presence of molecular oxygen.
- Hydroxamic acid adsorption on the quartz surface is enhanced by the presence of iron, facilitating stronger and more favorable molecular interactions with an adsorption energy of $-117\ kJ.mol^{-1}$, as demonstrated by *ab initio* simulations.

In summary, this study shows that •OH generation of coal-quartz differs based on the quartz content of metal impurities including iron. This study identifies key chemical additives, such as CMC, for effective inhibition of quartz toxicity. Atmospheric aging gradually mitigates •OH generation through the decay of surface siloxyl radicals.

Environmental implication

Quartz is a major component of coal and coal dust. Prolonged exposure to quartz dust can cause severe respiratory diseases, such as silicosis, and it is classified as a Group 1 carcinogen. Quartz is a key factor in the resurgence of pneumoconiosis among coal miners. This research investigates the surface chemistry of quartz samples associated with coals of various ranks and explores surface-modifying agents to reduce hydroxyl radical generation, thereby lowering particle toxicity. Our findings indicate that certain additives can effectively reduce coal-quartz toxicity, offering potential for minimizing health risks associated with respirable quartz and coal dust exposure.

CRediT authorship contribution statement

Eskanlou Amir: Writing – original draft, Visualization, Validation, Investigation, Formal analysis, Data curation. **Arnold Barbara J:** Writing – review & editing, Supervision, Resources, Project administration, Funding acquisition, Conceptualization.

Declaration of Competing Interest

The authors declare that they have no known competing financial interests or personal relationships that could have appeared to influence the work reported in this paper.

Acknowledgements

The authors acknowledge funding by the National Institute for Occupational Safety and Health (NIOSH) (NIOSH BAA: 75D301-21-R-71744). The Co-PIs, Sekhar Bhattacharyya (associate teaching professor) and Mohammad Rezaee (associate professor) at Penn State University Department of Energy and Mineral Engineering are recognized for their contribution to the proposal and guidance during this work. We also acknowledge the use of the Roar Collab supercomputer at the Penn State Institute for Computational and Data Sciences.

Appendix A. Supporting information

Supplementary data associated with this article can be found in the online version at doi:10.1016/j.jhazmat.2025.137873.

Data availability

Data will be made available on request.

References

[1] Arnold, C., 2016. A scourge returns: black lung in Appalachia. Natl Inst Environ Health Sci. https://doi.org/10.1289/ehp.124-A13.
[2] Cohen, R.A., Rose, C.S., Go, L.H.T., Zell-Baran, L.M., Almberg, K.S., Sarver, E.A., Lowers, H.A., et al., 2022. Pathology and mineralogy demonstrate respirable crystalline silica is a major cause of severe pneumoconiosis in US coal miners. Ann Am Thorac Soc 19 (9), 1469–1478. https://doi.org/10.1513/AnnalsATS.202109-1064OC.
[3] Zhang, R., Liu, S., Zheng, S., 2021. Characterization of nano-to-micron sized respirable coal dust: Particle surface alteration and the health impact. J Hazard Mater 413, 125447. https://doi.org/10.1016/j.jhazmat.2021.125447.
[4] Sarver, E., Keleş, Ç ., Afrouz, S.G., 2021. Particle size and mineralogy distributions in respirable dust samples from 25 US underground coal mines. Int J Coal Geol 247, 103851. https://doi.org/10.1016/j.coal.2021.103851.
[5] Sellaro, R., Sarver, E., Baxter, D., 2015. A standard characterization methodology for respirable coal mine dust using SEM-EDX. Resources. https://doi.org/10.3390/resources4040939.
[6] Schins, R.P.F., Borm, P.J.A., 1999. Mechanisms and mediators in coal dust induced toxicity: a review. Ann Occup Hyg 43 (1), 7–33. https://doi.org/10.1093/annhyg/43.1.7.
[7] Zazouli, M.A., Dehbandi, R., Mohammadyan, M., Aarabi, M., Dominguez, A.O., Kelly, F.J., Khodabakhshloo, N., Rahman, M.M., Naidu, R., 2021. Physicochemical properties and reactive oxygen species generation by respirable coal dust: implication for human health risk assessment. J Hazard Mater 405, 124185. https://doi.org/10.1016/j.jhazmat.2020.124185.
[8] Jomova, K., Raptova, R., Alomar, S.Y., Alwasel, S.H., Nepovimova, E., Kuca, K., Valko, M., Oct. 2023. Reactive oxygen species, toxicity, oxidative stress, and antioxidants: chronic diseases and aging. Arch Toxicol 97 (10), 2499–2574. https://doi.org/10.1007/s00204-023-03562-9.
[9] Cadet, J., Delatour, T., Douki, T., Gasparutto, D., Pouget, J.P., Ravanat, J.L., Sauvaigo, S., 1999. Hydroxyl radicals and DNA base damage. Mutat Res Mol Mech Mutagen 424 (1–2), 9–21. https://doi.org/10.1016/S0027-5107(99)00004-4.

[10] Kumar, P., Kalaiarasan, G., Porter, A.E., Pinna, A., Kłosowski, M.M., Demokritou, P., Chung, K.F., Pain, C., Arvind, D.K., Arcucci, R., Adcock, I.M., 2021. An overview of methods of fine and ultrafine particle collection for physicochemical characterization and toxicity assessments. Sci Total Environ 756. https://doi.org/10.1016/j.scitotenv.2020.143553.
[11] Dalal, N.S., Newman, J., Pack, D., Leonard, S., Vallyathan, V., 1995. Hydroxyl radical generation by coal mine dust: possible implication to coal workers' pneumoconiosis (CWP). Free Radic Biol Med 18 (1), 11–20. https://doi.org/10.1016/0891-5849(94)E0094-Y.
[12] Liu, T., Liu, S., 2020. The impacts of coal dust on miners' health: a review. Environ Res 190, 109849. https://doi.org/10.1016/j.envres.2020.109849.
[13] Harrington, A.D., Hylton, S., Schoonen, M.A.A., 2012. Pyrite-driven reactive oxygen species formation in simulated lung fluid: implications for coal workers' pneumoconiosis. Environ Geochem Health 34, 527–538. https://doi.org/10.1007/s10653-011-9438-7.
[14] Suarthana, E., Laney, A.S., Storey, E., Hale, J.M., Attfield, M.D., 2011. Coal workers' pneumoconiosis in the United States: regional differences 40 years after implementation of the 1969 federal coal mine health and safety act. Occup Environ Med 68 (12), 908–913. https://doi.org/10.1136/oem.2010.063594.
[15] Trechera, P., Moreno, T., Córdoba, P., Moreno, N., Zhuang, X., Li, B., Li, J., Shangguan, Y., Kandler, K., Dominguez, A.O., Kelly, F., Querol, X., 2020. Mineralogy, geochemistry and toxicity of size-segregated respirable deposited dust in underground coal mines. J Hazard Mater 399 (December 2019), 122935. https://doi.org/10.1016/j.jhazmat.2020.122935.
[16] Maeda, M., Nishimura, Y., Kumagai, N., Hayashi, H., Hatayama, T., Katoh, M., Miyahara, N., Yamamoto, S., Hirastuka, J., Otsuki, T., 2010. Dysregulation of the immune system caused by silica and asbestos. J Immunotoxicol 7 (4), 268–278. https://doi.org/10.3109/1547691X.2010.512579.
[17] Fubini, B., Areán, C.O., 1999. Chemical aspects of the toxicity of inhaled mineral dusts. Chem Soc Rev 28 (6), 373–381. https://doi.org/10.1039/a805639k.
[18] Fubini, B., 1998. Surface chemistry and quartz hazard. Ann Occup Hyg 42 (8), 521–530. https://doi.org/10.1093/annhyg/42.8.521.
[19] Pavan, C., Delle Piane, M., Gullo, M., Filippi, F., Fubini, B., Hoet, P., Horwell, C.J., Huaux, F., Lison, D., Lo Giudice, C., Martra, G., Montfort, E., Schins, R., Sulpizi, M., Wegner, K., Wyart-Remy, M., Ziemann, C., Turci, F., 2019. The puzzling issue of silica toxicity: are silanols bridging the gaps between surface states and pathogenicity? Part Fibre Toxicol 16 (1), 1–10. https://doi.org/10.1186/s12989-019-0315-3.
[20] Hall, N.B., Blackley, D.J., Halldin, C.N., Laney, A.S., 2019. Continued increase in prevalence of r-type opacities among underground coal miners in the USA. Occup Environ Med 76 (7), 479–481. https://doi.org/10.1136/oemed-2019-105691.
[21] Cohen, R.A., Petsonk, E.L., Rose, C., Young, B., Regier, M., Najmuddin, A., Abraham, J.L., Churg, A., Green, F.H., 2016. Lung pathology in US coal workers with rapidly progressive pneumoconiosis implicates silica and silicates. Am J Respir Crit Care Med 193 (6), 673–680. https://doi.org/10.1164/rccm.201505-1014OC.
[22] Doney, B.C., Blackley, D., Hale, J.M., Halldin, C., Kurth, L., Syamlal, G., Laney, A. S., 2020. Respirable coal mine dust at surface mines, United States, 1982–2017. Am J Ind Med 63 (3), 232–239. https://doi.org/10.1002/ajim.23074.
[23] Johann-Essex, V., Keles, C., Rezaee, M., Scaggs-Witte, M., Sarver, E., 2017. Respirable coal mine dust characteristics in samples collected in central and northern Appalachia. Int J Coal Geol 182, 85–93. https://doi.org/10.1016/j.coal.2017.09.010.
[24] Laney, A.S., Petsonk, E.L., Attfield, M.D., 2010. Pneumoconiosis among underground bituminous coal miners in the United States: is silicosis becoming more frequent? Occup Environ Med 67 (10), 652–656. https://doi.org/10.1136/oem.2009.047126.
[25] Cohen, R.A.C., 2010. Is the increasing prevalence and severity of coal workers' pneumoconiosis in the United States due to increasing silica exposure? Occup Environ Med 67 (10), 649–650. https://doi.org/10.1136/oem.2009.050096.
[26] Dos S Antao, V.C., Petsonk, E.L., Sokolow, L.Z., Wolfe, A.L., Pinheiro, G.A., Hale, J. M., Attfield, M.D., 2005. Rapidly progressive coal workers' pneumoconiosis in the United States: geographic clustering and other factors. Occup Environ Med 62 (10), 670–674. https://doi.org/10.1136/oem.2004.019679.
[27] Blackley, D.J., 2016. Resurgence of progressive massive fibrosis in coal miners—Eastern Kentucky, 2016. Mmwr Morb Mortal Wkly Rep 65. https://doi.org/10.15585/mmwr.mm6549a1.
[28] Kuempel E.D., Occupational exposure to respirable coal mine dust, 1995, ⟨https://stacks.cdc.gov/view/cdc/11239⟩..
[29] Barsan M.E., NIOSH pocket guide to chemical hazards, 2007, ⟨https://stacks.cdc.gov/view/cdc/21265⟩..
[30] Koskela, R.-S., Klockars, M., Laurent, H., Holopainen, M., 1994. Silica dust exposure and lung cancer. Scand J Work Environ Health 407–416. ⟨https://www.jstor.org/stable/40966286⟩.
[31] Poinen-Rughooputh, S., Rughooputh, M.S., Guo, Y., Rong, Y., Chen, W., 2016. Occupational exposure to silica dust and risk of lung cancer: an updated meta-analysis of epidemiological studies. BMC Public Health 16 (1), 1–17. https://doi.org/10.1186/s12889-016-3791-5.
[32] Wilbourn, J.D., McGregor, D.B., Partensky, C., Rice, J.M., 1997. IARC reevaluates silica and related substances. Environ Health Perspect 105 (7), 756–759 https://doi.org/10.1289%2Fehp.97105756.
[33] Ziemann, C., Escrig, A., Bonvicini, G., Ibáñez, M.J., Monfort, E., Salomoni, A., Creutzenberg, O., 2017. Organosilane-based coating of quartz species from the traditional ceramics industry: evidence of hazard reduction using in vitro and in vivo tests. Ann Work Expo Heal 61 (4), 468–480. https://doi.org/10.1093/annweh/wxx014.
[34] Schins, R.P.F., Duffin, R., Höhr, D., Knaapen, A.M., Shi, T., Weishaupt, C., Stone, V., Donaldson, K., Borm, P.J.A., 2002. Surface modification of quartz inhibits toxicity, particle uptake, and oxidative DNA damage in human lung epithelial cells. Chem Res Toxicol 15 (9), 1166–1173. https://doi.org/10.1021/tx025558u.
[35] Hair, M.L., 1975. Hydroxyl Groups on Silica Surface, Second Edi., 19. North-Holland Publishing Company. https://doi.org/10.1016/b978-0-7204-0419-7.50033-0.
[36] Pavan, C., Leinardi, R., Benhida, A., Ibouraadaten, S., Yakoub, Y., Brule, S. van den, Lison, D., Turci, F., Huaux, F., 2024. Short-and long-term pathologic responses to quartz are induced by nearly free silanols formed during crystal fracturing. Part Fibre Toxicol 21 (1), 1–13. https://doi.org/10.1186/s12989-024-00611-8.
[37] Narayanasamy, J., Kubicki, J.D., 2005. Mechanism of hydroxyl radical generation from a silica surface: molecular orbital calculations. J Phys Chem B 109 (46), 21796–21807. https://doi.org/10.1021/jp0543025.
[38] Jennings M., Flahive M., Review of the Health Effects associated with Exposure to Respirable Crystalline Silica in Coal Dust, ⟨https://www.coalservices.com.au⟩..
[39] Turci, F., Pavan, C., Leinardi, R., Tomatis, M., Pastero, L., Garry, D., Anguissola, S., Lison, D., Fubini, B., 2016. Revisiting the paradigm of silica pathogenicity with synthetic quartz crystals: The role of crystallinity and surface disorder. Part Fibre Toxicol 13 (1), 1–13. https://doi.org/10.1186/s12989-016-0136-6.
[40] Pavan, C., Fubini, B., Jan. 2017. Unveiling the variability of quartz hazard in light of recent toxicological findings. Chem Res Toxicol 30 (1), 469–485. https://doi.org/10.1021/acs.chemrestox.6b00409.
[41] Keleş, Ç ., Sarver, E., Dec. 2023. Respirable silica particles in coal mine dust: an image library dataset collected using scanning electron microscopy with energy dispersive X-ray spectroscopy. Data Brief 51, 109656. https://doi.org/10.1016/j.dib.2023.109656.
[42] Keles, C., Pokhrel, N., Sarver, E., 2022. A study of respirable silica in underground coal mines: sources. Minerals 12 (9), 1115. https://doi.org/10.3390/min12091115.
[43] Keles, C., Sarver, E., Dec. 2022. A study of respirable silica in underground coal mines: particle characteristics. Minerals 12 (12), 1555. https://doi.org/10.3390/min12121555.
[44] Elie, G., Pandey, R., Sarver, E., Dec. 2024. Direct-on-filter FTIR analysis of respirable crystalline silica: a field study to demonstrate utility for routine non-regulatory monitoring in coal mines. Min Metall Explor 41 (6), 2817–2831. https://doi.org/10.1007/s42461-024-01154-4.
[45] Donaldson, K.E.N., Borm, P.J.A., 1998. The quartz hazard: a variable entity. Ann Occup Hyg 42 (5), 287–294. https://doi.org/10.1093/annhyg/42.5.287.
[46] Das, M., Salinas, V., LeBoeuf, J., Khan, R., Jacquez, Q., Camacho, A., Hovingh, M., Zychowski, K., Rezaee, M., Roghanchi, P., Rubasinghege, G., 2023. A toxicological study of the respirable coal mine dust: assessment of different dust sources within the same mine. Minerals 13 (3), 433. https://doi.org/10.3390/min13030433.
[47] Chen, Z., Cheng, X., Wang, X., Ni, S., Yu, Q., Hu, J., Jan. 2024. Identification of core carcinogenic elements based on the age-standardized mortality rate of lung cancer in Xuanwei formation coal in China. Sci Rep 14 (1), 232. https://doi.org/10.1038/s41598-023-49975-5.
[48] Salopek, B., Krasic, D., Filipovic, S., 1992. Measurement and application of zeta-potential. Rud Zb 4 (1), 147. ⟨https://hrcak.srce.hr/file/39012?ref=Guzels.TV⟩.
[49] Jimenez-Relinque, E., Castellote, M., 2015. Quantification of hydroxyl radicals on cementitious materials by fluorescence spectrophotometry as a method to assess the photocatalytic activity. Cem Concr Res 74, 108–115. https://doi.org/10.1016/j.cemconres.2015.04.011.
[50] Náfrádi, M., Farkas, L., Alapi, T., Hernádi, K., Kovács, K., Wojnárovits, L., Takács, E., 2020. Application of coumarin and coumarin-3-carboxylic acid for the determination of hydroxyl radicals during different advanced oxidation processes. Radiat Phys Chem 170, 108610. https://doi.org/10.1016/j.radphyschem.2019.108610.
[51] Jain, A., Ong, S.P., Hautier, G., Chen, W., Richards, W.D., Dacek, S., Cholia, S., Gunter, D., Skinner, D., Ceder, G., Persson, K.A., 2013. Commentary: the materials project: a materials genome approach to accelerating materials innovation. APL Mater 1 (1), 11002. https://doi.org/10.1063/1.4812323.
[52] Jia, J., Liang, Y., Tsuji, T., Miranda, C.R., Masuda, Y., Matsuoka, T., 2019. Ab initio molecular dynamics study of carbonation and hydrolysis reactions on cleaved quartz (001) surface. J Phys Chem C 123 (8), 4938–4948. https://doi.org/10.1021/acs.jpcc.8b12089.
[53] Ikuta, D., Kawame, N., Banno, S., Hirajima, T., Ito, K., Rakovan, J.F., Downs, R.T., Tamada, O., 2007. First in situ X-ray identification of coesite and retrograde quartz on a glass thin section of an ultrahigh-pressure metamorphic rock and their crystal structure details. Am Mineral 92 (1), 57–63. https://doi.org/10.2138/am.2007.2228.
[54] Georg K.VASP Group, Theoretical Physics Departments, Vienna, Retrieved Febr., vol. 21, 2011..
[55] Hettiarachchi, E., Paul, S., Cadol, D., Frey, B., Rubasinghege, G., 2018. Mineralogy controlled dissolution of uranium from airborne dust in simulated lung fluids (SLFs) and possible health implications. Environ Sci Technol Lett 6 (2), 62–67. https://doi.org/10.1021/acs.estlett.8b00557.
[56] Nolan, R.P., Langer, A.M., Harington, J.S., Oster, G., Selikoff, I.J., 1981. Quartz hemolysis as related to its surface functionalities. Environ Res 26 (2), 503–520. https://doi.org/10.1016/0013-9351(81)90226-7.
[57] Michael, H.L., Williams, D.J.A., 1984. Electrochemical properties of quartz. J Electroanal Chem Interfacial Electrochem 179 (1–2), 131–139. https://doi.org/10.1016/S0022-0728(84)80282-X.
[58] Castranova, V., Vallyathan, V., Ramsey, D.M., McLaurin, J.L., Pack, D., Leonard, S., Barger, M.W., Ma, J.Y., Dalal, N.S., Teass, A., 1997. Augmentation of pulmonary

reactions to quartz inhalation by trace amounts of iron-containing particles. Environ Health Perspect 105 (5), 1319–1324. https://doi.org/10.1289/ehp.97105s51319.
[59] Eskanlou, A., Arnold, B.J., 2024. An evaluation of pyrite as a component of respirable coal dust. J Hazard Mater 477, 135340. https://doi.org/10.1016/j.jhazmat.2024.135340.
[60] Orem, W.H., Finkelman, R.B., 2003. Coal formation and geochemistry, 7. https://doi.org/10.1016/B0-08-043751-6/07097-3.
[61] Dai, S., Finkelman, R.B., French, D., Hower, J.C., Graham, I.T., Zhao, F., 2021. Modes of occurrence of elements in coal: a critical evaluation. Earth-Sci Rev 222, 103815 https://doi.org/10.1016/j.earscirev.2021.103815. 103815, 2021.
[62] Huang, X., 2003. Iron overload and its association with cancer risk in humans: evidence for iron as a carcinogenic metal. Mutat Res Mol Mech Mutagen 533 (1–2), 153–171. https://doi.org/10.1016/j.mrfmmm.2003.08.023.
[63] Beccia M.R., Hydroxamic acids interactions with metals in aqueous and micellar media: a mechanistic study of complexation reactions and metallacrown formation. Università degli studi di Pisa, 2012, ⟨https://theses.hal.science/tel-00967266⟩..
[64] Albright, T.A., Burdett, J.K., Whangbo, M.-H., 2013. Orbital interactions in chemistry. John Wiley & Sons. https://doi.org/10.1002/9781118558409.
[65] Nduwa-Mushidi, J., Anderson, C.G., Mar. 2017. Surface chemistry and flotation behaviors of monazite–apatite–ilmenite–quartz–rutile–zircon with octanohydroxamic acid. J Sustain Metall 3 (1), 62–72. https://doi.org/10.1007/s40831-016-0114-0.
[66] Gulumian, M., 2005. An update on the detoxification processes for silica particles and asbestos fibers: successess and limitations. J Toxicol Environ Heal Part B 8 (6), 453–483. https://doi.org/10.1080/10937400590952547.
[67] Končić, M.Z., Barbarić, M., Perković, I., Zorc, B., 2011. Antiradical, chelating and antioxidant activities of hydroxamic acids and hydroxyureas. Molecules 16 (8), 6232–6242. https://doi.org/10.3390/molecules16086232.
[68] Tsyganenko, A.A., Storozheva, E.N., Manoilova, O.V., Lesage, T., Daturi, M., Lavalley, J.-C., 2000. Brønsted acidity of silica silanol groups induced by adsorption of acids. Catal Lett 70, 159–163. https://doi.org/10.1023/A:1018845519727.
[69] Castranova, V., Vallyathan, V., 2000. Silicosis and coal workers' pneumoconiosis. Environ Health Perspect 108 (. 4), 675–684. https://doi.org/10.1289/ehp.00108s4675.
[70] Segneanu, A.E., Gozescu, I., Dabici, A., Sfirloaga, P., Szabadai, Z., 2012. Organic compounds FT-IR spectroscopy, 145. InTech Rijeka, Croatia. https://doi.org/10.5772/50183.
[71] Vallyathan, V., Shi, X., Dalal, N.S., Irr, W., Castranova, V., 1988. Generation of free radicals from freshly fractured silica dust. Am Rev Respir Dis 138 (5), 1213–1219. https://doi.org/10.1164/ajrccm/138.5.1213.
[72] Petushkov, A., Ndiege, N., Salem, A.K., Larsen, S.C., 2010. Toxicity of silica nanomaterials: zeolites, mesoporous silica, and amorphous silica nanoparticles. Advances in Molecular Toxicology. Elsevier, pp. 223–266. https://doi.org/10.1016/S1872-0854(10)04007-5.
[73] Dalai N.S., Suryan M.M., Jafari B., Shi X., Vallyathan V., and Green F.H.Y. , Electron spin resonance detection of reactive free radicals in fresh coal dust and quartz dust and its implications to pneumoconiosis and silicosis, in Proceedings of the International Symposium of Respirable Dusts in the Mineral Industries. University Park, PA: Pennsylvania State University, 1986, pp. 25–29..
[74] Vallyathan, S., Shi, V., 1997. The role of oxygen free radicals in occupational and environmental lung diseases. Env. Heal. Perspect, vol. 1, pp. 65–177 Environ Health Perspect 105 (1), 165–178. https://doi.org/10.1289/ehp.97105s1165.
[75] Vallyathan, V., Castranova, V., Pack, D., Leonard, S., Shumaker, J., Hubbs, A.F., Shoemaker, D.A., Ramsey, D.M., Pretty, J.R., McLaurin, J.L., 1995. Freshly fractured quartz inhalation leads to enhanced lung injury and inflammation. Potential role of free radicals. Am J Respir Crit Care Med 152 (3), 1003–1009. https://doi.org/10.1164/ajrccm.152.3.7663775.
[76] Castranova, V., Pailes, W.H., Dalai, N.S., Miles, P.R., Bowman, L., Vallyathan, V., Pack, D., Weber, K.C., Hubbs, A., Schwegler-Berry, D., 1996. Enhanced pulmonary response to the inhalation of freshly fractured silica as compared with aged dust exposure. Appl Occup Environ Hyg 11 (7), 937–941. https://doi.org/10.1080/1047322X.1996.10389993.
[77] Mai, A., 2009. Hydroxamic acids: biological properties and potential uses as therapeutic agents. PATAI'S Chem Funct Groups. https://doi.org/10.1002/9780470682531.pat0515.
[78] Winston, A., Kirchner, D., 1978. Hydroxamic acid polymers. Effect of structure on the selective chelation of iron in water. Macromolecules 11 (3), 597–603. https://doi.org/10.1021/ma60063a033.